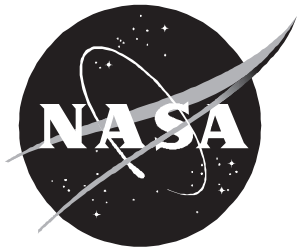

NASA Technical Paper 3533

NUCFRG2: An Evaluation of the Semiempirical Nuclear Fragmentation Database

J. W. Wilson
Langley Research Center • Hampton, Virginia

R. K. Tripathi
University of Southern Illinois • Carbondale, Illinois

F. A. Cucinotta and J. L. Shinn
Langley Research Center • Hampton, Virginia

F. F. Badavi
Christopher Newport University • Newport News, Virginia

S. Y. Chun
Old Dominion University • Norfolk, Virginia

J. W. Norbury
University of Wisconsin • LaCrosse, Wisconsin

C. J. Zeitlin, L. Heilbronn, and J. Miller
Lawrence Berkeley Laboratory • Berkeley, California

National Aeronautics and Space Administration
Langley Research Center • Hampton, Virginia 23681-0001

October 1995

Available electronically at the following URL address: http://techreports.larc.nasa.gov/ltrs/ltrs.html

Printed copies available from the following:

NASA Center for AeroSpace Information
800 Elkridge Landing Road
Linthicum Heights, MD 21090-2934
(301) 621-0390

National Technical Information Service (NTIS)
5285 Port Royal Road
Springfield, VA 22161-2171
(703) 487-4650

Abstract

A semiempirical abrasion-ablation model has been successful in generating a large nuclear database for the study of high charge and energy (HZE) ion beams, radiation physics, and galactic cosmic ray shielding. The version reported herein has coulomb trajectory corrections, improved transmission factors, improved surface energy corrections, and light fragment emission was added. The cross sections that are generated are compared with measured HZE fragmentation data from various experimental groups. A research program for improvement of the database generator is discussed.

Introduction

An adequate and reliable nuclear database that assesses the quality of heavy ion beams for various technological efforts is needed. For example, the nuclear fragmentation properties of shielding materials can alter the protection of astronauts by an order of magnitude through the selection of appropriate shield materials (refs. 1 and 2). The radiation quality of heavy ions, which is related to the ability to cause biological injury, is an essential parameter in high altitude commercial aviation, radiotherapy, microelectronic signal processing, and information storage. Understanding single event upset damage to microelectronic systems is becoming more important as more aircraft and spacecraft control functions are handled by microprocessors. This damage is of special concern for miniature spacecraft in which reduced telemetry requires intensive onboard processing by low power microprocessors with large memory. Such small scale devices are very sensitive to single event upsets and evaluation of onboard shield worth is critical to an adequate design. The specification of the nuclear fragmentation cross sections is critical in all these applications.

Over the years the theoretical description of nuclear fragmentation in heavy ion collisions has been described with abrasion-ablation models (refs. 3 to 11 and recent work by Cucinotta, Townsend, and Wilson of Langley Research Center). In these models, fragmentation occurs in two stages. In the fast abrasion stage, the projectile and the target overlap and matter is sheared away from both nuclei. The remnants of the colliding nuclei are called the prefragments (projectile or target) and are assumed to be left in a state of excitation. The ablation stage is the description of the decay of the prefragment nuclei. The emphasis of these models is typically the prediction of inclusive mass yields of the final fragments that are observed. In the semiempirical descriptions of these reactions (refs. 3 to 6), the overlap volume of projectile and target is estimated by using a classical approach. The excitation energy of the prefragments is estimated by using a surface distortion model with correction terms and energy transfer across the interface of the interaction zone. These models provide reasonable overall agreement with measured data; however, they lack a description of nuclear structure effects and a description of the nuclear diffuseness related to skin thickness. A fundamental and more complex problem is the degree to which the distribution of levels of prefragment nuclei must be considered to provide the correct description (ref. 5).

Hüfner, Schäfer, and Schürmann used the Glauber model in a first attempt at formulating a quantum mechanical abrasion-ablation model (ref. 7). In this model, closure is made on the final states of the target in describing the projectile fragmentation and the unobserved nucleons abraded from the projectile. Energy conservation is also ignored and a final closure approximation is assumed for the prefragment states that occur following the removal of a fixed number of nucleons. The advantageous factorization properties in the Glauber model of the nuclear amplitude then allow closed-form expressions for the abrasion cross sections to be found. The Glauber model of the abrasion cross section can then be shown to correspond closely to the semiempirical models when the abrasion cross section for a given product relates to the volume of the projectile and the target removed in their overlap. A study of the closed-form expression for the nuclear absorption cross section in the eikonal form of the first-order optical potential model led to a recasting of the abrasion model as an optical model by using the binomial distribution (refs. 8, 9, 12, and 13). A comparison of the abrasion cross sections (ref. 7) with the optical models (refs. 8, 9, and 12) reveals that the two differ only by the assumptions of coherence and closure in the projectile intermediate states. The optical models being preferred for the sum rule on the abrasion cross sections to satisfy unitarity.

The Glauber model or the optical model of abrasion began to employ sophisticated evaporation or cascade/evaporation codes to describe the ablation stage. These codes rely on a correct average excitation energy to be used to start the evaporation process. A major shortcoming in the physical description results from the use of closure on the prefragment final states in the Glauber model (ref. 7). In the Glauber model, all information on the distribution of the actual levels excited from abrasion in the prefragment state is lost and is replaced by an average state that is described uniquely by the abrasion cross section and average excitation energy. For light prefragments (mass number (A) is less than 16) where nuclear structure effects are large and resonance levels separated by several MeV, the use of an average prefragment state is highly questionable.

The use of a cascade model in the ablation stage is also noted. In the abrasion stage, nucleons in the projectile are knocked into the continuum by the target. These escaping nucleons will multiple scatter inside the projectile and cause further nucleon knockout. This process may be described as final state interaction (FSI) with the Moller operator and is expected to be highly dependent on the trajectory of the initial cascading nucleon (ref. 14). In the optical model (ref. 12) and the semiempirical model (refs. 5 and 6), a final state interaction correction to the prefragment excitation energy has been used to mimic the cascade effect of projectile knockouts. It is unclear whether the cascade effects described by the Monte-Carlo codes for describing ablation are distinct from the FSI corrections that describe prefragment nuclei. It was further found in the semiempirical model that statistical fluctuations in the FSI correction must be considered (ref. 5).

In a more recent formulation of the abrasion-ablation model that uses the Glauber amplitude, three major improvements are made (refs. 10 and 11 and recent work by Cucinotta, Townsend, and Wilson of Langley Research Center). First, energy conservation is treated in describing nuclear abrasion. Second, the treatment of the excitation of specific levels in the prefragments is considered for the first time. Here the prefragment excitation is considered as a core excitation during the knockout stage of abrasion. By using fractional parentage coefficients to couple nucleons to the core (prefragment) in the projectile ground state, we expect that for many nuclei the complex configurations of the nuclear ground state that result in virtual states of relative excitation are such that the core excitation is dominated by diagonal transitions to excited states of the prefragment. As the number of nucleons lost in abrasion becomes large, the use of parentage coefficients to form the prefragment level spectrum will become intractable. For many nucleon knockouts, off-diagonal coupling is expected to become more dominant and statistical methods will become necessary to determine the distribution of prefragment levels. The preequilibrium models developed by Feshbach et al. (ref. 15), Griffin (ref. 16), and Tamura, Udagawa, and Lenske (ref. 17) may be amenable to the description of the heating of prefragment nuclei in heavy ion collisions. The third development in the reformulation of the abrasion-ablation model is the description of cluster knockout in nuclear abrasion. This description allows the treatment of nuclear structure effects in nuclear abrasion, which is important for many projectile and target nuclei of interest (C, O, and Ne). The reformulation also considers the momentum distribution for nucleon production from abrasion (ref. 18) as well as ablation (ref. 19). Although this more systematic approach will ultimately meet the need for a high quality nuclear database, current interaction studies rely on the semiempirical model.

The genesis of the semiempirical model is in the abrasion-ablation model of Bowman, Swiatecki, and Tsang (ref. 4) as discussed in references 5 and 6. In the development of the model, the transmission factors of a projectile and target were averaged and included to account for the mean free path in nuclear matter (ref. 6). Then, a semiempirical higher order correction was given to the surface deformation energy of the abrasion products (ref. 6) and the energy transfer across the interaction zone boundary was treated as a two-valued distribution (ref. 5). The final charge distribution of the fragmentation products was approximated by Rudstam's formalism (ref. 6). The available experimental nuclear fragmentation data were very limited at the time of the first reporting of the model (ref. 6). The model agreed with experimental data to the extent that the experimentalists agreed among themselves.

Since the inception of the NUCFRG model, additional experimental fragmentation cross sections (refs. 20 to 23) and thick target fluence data (refs. 24 and 25) have become available for validation of the database. Incremental improvements have been made by including the coulomb dissociation contribution (ref. 26), an energy-dependent nuclear mean free path (ref. 27) based on the analysis of Dymarz and Kohmura (ref. 28), and the nuclear radii extracted from experimental charge distributions (ref. 27). These improvements were included in the publicly released version of the HZEFRG1 code (ref. 27). In addition to these improvements, the version of the code described herein

also includes the following. A coulomb trajectory correction that includes the effects of an energy downshift has been added (ref. 29). The transmission factor is evaluated at the maximum overlap in the interaction zone. The spectator nucleons in the interaction zone are now assumed to be poorly bound to the spectators of the abraded fragment outside the interaction zone and undergo preequilibrium emission. A unitarity correction is made for targets with $A > 63$. Finally, a correction to the semiempirical excess surface distortion energy is made for light projectiles.

In the report presented herein, the model database is compared with available experimental data. Weaknesses within the model are thereby uncovered and a research program for database improvement is outlined.

Semiempirical Fragmentation Model

The equation of motion for a low energy ion in a nuclear coulomb field is given by energy conservation as

$$E_{\text{tot}} = \frac{1}{2}\mu\dot{r}^2 + \frac{\ell^2}{2\mu r^2} + \frac{Z_P Z_T e^2}{r} \tag{1}$$

where E_{tot} is the total energy in the center of mass, r is the relative distance between the charge centers with time derivative $\dot{r}, \mu$ is the reduced mass, ℓ is the angular momentum, Z_P and Z_T are the atomic numbers of the projectile nucleus and target nucleus, respectively, and e is the electric charge. (That is, $e^2 = 2R_y a_o$, where R_y is the Rydberg constant and a_o is the Bohr radius.) The angular momentum is given as

$$\ell^2 = 2\mu E_{\text{tot}} b^2 \tag{2}$$

The distance of closest approach is given by equation (1) for $\dot{r} = 0$ as

$$E_{\text{tot}} = \frac{E_{\text{tot}} b^2}{r^2} + \frac{Z_P Z_T e^2}{r} \tag{3}$$

which is written as

$$b^2 = r(r - r_m) \tag{4}$$

where

$$r_m = \frac{Z_P Z_T e^2}{E_{\text{tot}}} \tag{5}$$

Note that r_m is the distance of closest approach for zero impact parameter.

At a given impact parameter, there is a distance of closest approach r for which the interaction takes place. When r is large, the interaction is dominated by coulomb excitation, which is discussed by Norbury et al. (ref. 30). At smaller distances, the overlap of the nuclear densities strongly interact and mass is removed from the projectile and the target.

Abrasion Process Description

The strength of the interaction varies over the interaction zone. The projected interaction potential on the impact plane is given as

$$\int V(\mathbf{R} + \mathbf{z})\, d\mathbf{z} \approx \sigma \rho_P\, C_P(\mathbf{R})\, \rho_T\, C_T(\mathbf{R}) \tag{6}$$

where $\mathbf{R}$ is a position vector in the impact plane, $\mathbf{z}$ is the longitudinal position component, σ is the two-body cross section that includes Pauli blocking, ρ_P and ρ_T are the projectile and target mass density, respectively, and $C_P(\mathbf{R})$ and $C_T(\mathbf{R})$ are the projectile and target chord, respectively, at position $\mathbf{R}$ along $\mathbf{z}$. (See ref. 31.) The amount of nuclear material removed from the projectile in the collision at a given impact separation is the volume of the overlap region times an attenuation factor that is evaluated at the maximum product of the chords in equation (6). The formula for the number of participating projectile constituents in the interaction zone is

$$\Delta_{\text{abr}} = F A_P [1 - \exp(-C_T/\lambda)] \tag{7}$$

where A_P is projectile mass number, λ is mean free path, and C_T is the value of $C_T(\mathbf{R})$ that maximizes equation (6) and is given for $r_T > r_P$ as

$$C_T = \begin{cases} 2\sqrt{r_T^2 - x^2} & x > 0 \\ 2\sqrt{r_T^2 - r^2} & x \le 0 \end{cases} \tag{8}$$

where

$$x = (r_P^2 + r^2 - r_T^2)/(2r) \tag{9}$$

and r_P and r_T are the projectile and target radius, respectively, and are related to the root-mean-square charge radius (r_{rms}) of electron scattering $\left(r_j \approx 1.29\sqrt{r_{\text{rms}}^2 - 0.84^2}\right)$ (ref. 31). When $r_P > r_T$, the chord C_T is given as

$$C_T = \begin{cases} 2\sqrt{r_T^2 - x^2} & x > 0 \\ 2r_T & x \le 0 \end{cases} \tag{10}$$

in which

$$x = (r_T^2 + r^2 - r_P^2)/(2r) \tag{11}$$

The quantity F in equation (7) is the fraction of the projectile in the interaction zone as given in the

appendix (refs. 5, 6, 32, and 33). (The b in ref. 5 is replaced by the r in the equations presented herein.) The number of projectile spectator constituents in the interaction zone is given as

$$\Delta_{\text{spc}} = A_P F \ \exp(-C_T/\lambda) \tag{12}$$

The spectator constituents are assumed to be only loosely bound to the projectile constituents outside the interaction zone. The nuclear mean free path is taken as

$$\lambda = 16.6/E^{0.26} \tag{13}$$

where E is the projectile energy in MeV/nucleon. (See refs. 27 and 28.) The charge ratio of the removed nucleons is assumed to be that of the initial projectile nucleus, an assumption that ignores polarization effects.

Surface Distortion and Collisional Excitation

The projectile constituents outside the interaction zone (spectators) retain the same relation among themselves after the collision as before the collision. (This retention of relationship is a sudden approximation that is strictly applicable at higher energies.) The mass removed by the interaction has altered the overall stability of the spectators. This instability is related to the reduced binding energy when the nuclear surface is other than its minimum energy spherical configuration.

The excess surface area is given as

$$\Delta S = 4\pi r_P^2[1 + P - (1 - F)^{2/3}] \tag{14}$$

The functions F and P are defined in the appendix. (See ref. 32.) For small surface distortions ΔS in units of fm^2, the excitation energy E'_S in units of MeV is approximated by

$$E'_S = 0.95\,\Delta S \tag{15}$$

At the impact separations $r \ll r_P + r_T$, the projectile spectator group is left far from equilibrium and the 0.95 MeV/fm^2 coefficient requires correction that is taken herein as a semiempirical parameter f given by

$$f = 1 + 5F + [1500 - 320(A_P - 12)]\,F^3 \tag{16}$$

where the quantity in the square brackets is limited to values between 0 and 1500. The cubic coefficient F^3 provides a correction for light projectiles that are unstable because of large surface distortions. The semiempirical surface excitation energy is then

$$E_S = E'_S\, f \tag{17}$$

Note that the correction factor approaches 1 as Δ_{abr} becomes small. As before, we assume that fragments with a mass number of 5 are unbound, 90 percent of fragments with a mass number of 8 are unbound, and 50 percent of fragments with a mass number of 9 are unbound.

A second source of excitation energy is the transfer of kinetic energy of relative motion across the intersecting boundaries of the two ions. The rate of energy loss of a nucleon when passing through nuclear matter is taken as 13 MeV/fm (ref. 34). The energy deposit is assumed to be symmetrically dispersed about the azimuth so that at the interface 6.5 MeV/fm per nucleon is the average rate of energy transferred into excitation energy. This energy is transferred in single particle collisions. In half the events, the energy is transferred to excitation energy of the projectile and in the remaining events, the projectile excitation energy remains unchanged. The estimate of this contribution is made by using the length of the longest chord C_ℓ in the projectile surface interface. This chord length is the maximum distance traveled by any target constituent through the projectile interior and is given by

$$C_\ell = \left\{ \begin{array}{ll} 2(r_P^2 + 2rr_T - r^2 - r_T^2)^{1/2} & (r > r_T) \\ 2r_P & (r \le r_T) \end{array} \right\} \tag{18}$$

The number of other target constituents in the participant and spectator interface may be found by estimating the maximum chord transverse to the projectile velocity that spans the projectile surface interface C_t which is given by

$$C_t = 2(r_P^2 - b_P^2)^{1/2} \tag{19}$$

where

$$b_P = (r_P^2 + r^2 - r_T^2)/(2r) \tag{20}$$

The total excitation energy transferred across the participant and spectator interface is then

$$E'_x = 13\,C_\ell + \frac{1}{3}\ 13\,C_\ell(C_t - 1.5) \tag{21}$$

where the second term contributes only if $C_t >$ 1.5 fm. The effective longitudinal chord length for these remaining nucleons is assumed to be one third the maximum chord length.

Nuclear Ablation

The decay of highly excited nuclear states is dominated by heavy particle emission. In the present

model, a nucleon is assumed to be removed for every 10 MeV of excitation energy and is determined by

$$\Delta_{\mathrm{abl}} = (E_s + E_x)/10 + \Delta_{\mathrm{spc}} \tag{22}$$

where Δ_{spc} are the loosely bound projectile spectators in the interaction zone that are emitted prior to the equilibrium deexcitation process. (See ref. 4.) In accordance with the previously discussed directionality of the energy transfer, the E_x is double valued as

$$E_x = \left\{ \begin{array}{ll} E'_x & \left(P_x = \frac{1}{2}\right) \\ 0 & \left(P_{\bar{x}} = \frac{1}{2}\right) \end{array} \right\} \tag{23}$$

where P_j is the corresponding probability of occurrence for each value of E_x in the collision.

Nuclear Abrasion-Ablation Model

The number of nucleons removed through the abrasion-ablation process is given as a function of impact parameter b as

$$\Delta A = \Delta_{\mathrm{abr}}(b) + \Delta_{\mathrm{abl}}(b) \tag{24}$$

The impact parameter is related to the impact separation r by equation (4) for a coulomb trajectory.

A second correction to the trajectory calculation comes from the transfer of kinetic energy into binding energy during the release of particles from the projectile. (Obviously, energy is also lost in releasing particles from the target, which we do not yet calculate.) The total kinetic energy in passing through the reaction zone is reduced to

$$E_f = E_i - 10\ \Delta A \tag{25}$$

which assumes that 10 MeV is the average binding energy. The kinetic energy used in the closest approach calculation is the average of the initial and the final energies and is given as

$$E_{\mathrm{tot}} = \frac{1}{2}(E_i + E_f) = E_i - \frac{1}{2}(10\ \Delta A) \tag{26}$$

Obviously, E_{tot} as given by equation (26) is very crude and substantial improvements can be made. The values of ΔA for carbon projectiles on a copper target and for copper projectiles on a carbon target are shown in figure 1 for high energies. A real collision would be given by a statistical distribution between the limits shown by these two curves. The average event will be calculated as if the two extremes occurred with equal probability as noted in equation (23).

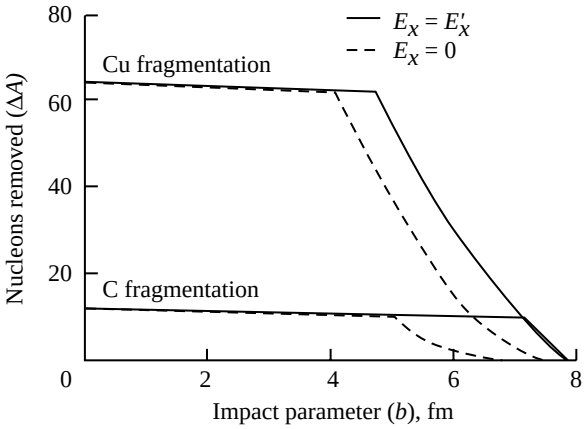

Figure 1. Nucleon removal number as a function of impact parameter in carbon-copper collisions.

The nuclear fragmentation cross sections discussed herein are approximated as the abrasion-ablation model of Bowman, Swiatecki, and Tsang (ref. 4). The cross section for removal of ΔA nucleons is estimated as

$$\sigma(\Delta A) = \pi b_2^2 - \pi b_1^2 \tag{27}$$

where b_2 is the impact parameter for which the volume of intersection of the projectile contains Δ_{abr} nucleons and the resulting excitation energies release Δ_{abl} additional nucleons at the rate of 1 nucleon for every 10 MeV of excitation so that

$$\Delta_{\mathrm{abr}}(b_2) + \Delta_{\mathrm{abl}}(b_2) = \Delta A - \frac{1}{2} \tag{28}$$

and similarly for b_1

$$\Delta_{\mathrm{abr}}(b_1) + \Delta_{\mathrm{abl}}(b_1) = \Delta A + \frac{1}{2} \tag{29}$$

The charge distributions of the final projectile fragments are strongly affected by nuclear stability. We expect that the charge distribution given by Rudstam (ref. 35) for a given $\sigma(\Delta A)$ to be reasonably correct as

$$\sigma(A_F, Z_F) = F_1 \exp\left[-R|Z_F - SA_F + TA_F^2|^{3/2}\right] \sigma(\Delta A) \tag{30}$$

where the values of $R = 11.8/A_F^D$, $D = 0.45$, $S = 0.486$, and $T = 3.8 \times 10^{-4}$ are taken from Rudstam and F_1 is a normalizing factor so that

$$\sum_{Z_F} \sigma(A_F, Z_F) = \sigma(\Delta A) \tag{31}$$

The formula of Rudstam for $\sigma(\Delta A)$ was not used because his ΔA dependence is too simple and is not useful for heavy targets. For fragments with a mass of 9, the cross sections were reduced by a factor of 2.6, and for fragments with a mass of 7, cross sections were increased by a factor of 1.25 and distributed between ^{7}Li and ^{7}Be with factors of 0.52 and 0.48, respectively.

The charge of the removed nucleons ΔZ is calculated according to charge conservation

$$\Delta Z = Z_P - Z_F \tag{32}$$

where Z_F is the charge of the fragment and Z_P is the charge of the projectile. The charge is divided according to the following rules among the nucleons and the light nuclei produced by the interaction. The abraded nucleons are those removed from the portion of projectile in the overlap region. Therefore, the abraded nucleon charge is assumed to be proportional to the charge fraction of the projectile nucleus and is given as

$$Z_{\rm abr} = Z_P \Delta_{\rm abr}/A_P \tag{33}$$

This assumption, of course, ignores the charge separation due to the giant dipole resonance model of Morrissey et al. (ref. 33). The charge release in the ablation is then given as

$$Z_{\rm abl} = \Delta Z - Z_{\rm abr} \tag{34}$$

which conserves the remaining charge. Similarly, mass is conserved to obtain $A_{\rm abl}$.

The alpha particle is unusually tightly bound in comparison to other nucleon arrangements. Because of this unusually tight binding, the helium production is maximized in the ablation process as

$$N_\alpha = [{\rm Int}(Z_{\rm abl}/2), {\rm Int}(A_{\rm abl}/4)]_{\rm minimum} \tag{35}$$

where ${\rm Int}(x)$ denotes the integer part of x. The other light isotopes are likewise maximized from the remaining ablated mass and charge numbers in the order of decreasing binding energy. The number of protons produced is given by charge conservation as

$$N_p = Z_{\rm abl} - \sum_i Z_i N_i \tag{36}$$

Similarly, mass conservation requires the number of neutrons produced to be

$$N_n = A_{\rm abl} - N_p - \sum_i A_i N_i \tag{37}$$

where the term i ranges over the mass numbers 2, 3, and 4 for ablated particles.

The calculation is performed for $\Delta A = 1$ to $\Delta A = A_P - 1$ for which the cross section associated with $\Delta A > A_P - 0.5$ is missed. This missed region corresponds to the central collisions for which it is assumed that the projectile disintegrates into single nucleons if $r_P < r_T$ then

$$N_p = Z_P \tag{38}$$

and

$$N_n = A_P - Z_P \tag{39}$$

Otherwise, this missed region is ignored. The energetic target fragments are being ignored as well as the mesonic components. The peripheral collisions with $\Delta A < 0.5$ are also missing. The most important process in these collisions with large impact separations will be the coulomb dissociation process (ref. 30).

Electromagnetic Dissociation

The total electromagnetic cross section for one nucleon removal that results from electric dipole ($E1$) and electric quadrupole ($E2$) interaction is written as

$$\begin{aligned}\sigma_{\rm em} &= \sigma_{E1} + \sigma_{E2} \\ &= \int \left[N_{E1}(E)\sigma_{E1}(E) + N_{E2}(E)\,\sigma_{E2}(E)\right] dE\end{aligned} \tag{40}$$

where the virtual photon spectra of energy E produced by the target nucleus are given by

$$N_{E1}(E) = \frac{1}{E}\,\frac{2}{\pi}\,Z^2\alpha\,\frac{1}{\beta^2}\left[\xi K_0 K_1 - \frac{1}{2}\,\xi^2\beta^2(K_1^2 - K_0^2)\right] \tag{41}$$

for the dipole field and by

$$\begin{aligned}N_{E2}(E) = \frac{1}{E}\,\frac{2}{\pi}\,Z^2\alpha\,\frac{1}{\beta^4}\Bigg[&2(1-\beta^2)\,K_1^2 \\ &+ \xi(2-\beta^2)^2\,K_0 K_1 - \frac{1}{2}\,\xi^2\beta^2(K_1^2 - K_0^2)\Bigg]\end{aligned} \tag{42}$$

where α is the fine structure constant for the quadrupole field. (See ref. 36.) The terms $\sigma_{E1}(E)$ and $\sigma_{E2}(E)$ are the corresponding photonuclear reaction cross sections for the fragmenting projectile nucleus. The terms K_0 and K_1 in the expression for N_{E1} and N_{E2} are modified Bessel functions of the second kind and are also functions of the parameter ξ with

$$\xi = \frac{2\pi E b_{\rm min}}{\gamma\beta\hbar c} \tag{43}$$

where E is the virtual photon energy, $b_{\min}$ is the minimum impact parameter below which the collision dynamics are dominated by nuclear interactions (rather than electromagnetic (EM) interactions), β is the speed of the target (measured from the projectile rest frame) as a fraction of the speed of light c, $\hbar$ is Planck's constant, and γ is the Lorentz factor from special relativity that is given by $\gamma = (1 - \beta^2)^{-1/2}$. The minimum impact parameter is given by

$$b_{\min} = (1 + x_d)\ b_c + \frac{\pi \alpha_0}{2\gamma} \tag{44}$$

where $x_d = 0.25$ and

$$\alpha_0 = \frac{Z_P Z_T e^2}{m_0 \beta^2 c^2} \tag{45}$$

allows for deviation of the trajectory from a straight line (ref. 37). The critical impact parameter for single nucleon removal is

$$b_c = 1.34 \left[A_P^{1/3} + A_T^{1/3} - 0.75 \left(A_P^{1/3} + A_T^{1/3} \right) \right] \tag{46}$$

where b_c is in units of fm and A_P and A_T are the projectile and the target nucleon mass numbers, respectively.

The photonuclear cross sections $\sigma_{E1}(E)$ and $\sigma_{E2}(E)$ are Lorentzian shaped and somewhat sharply peaked in energy. Therefore, the photon spectral functions can be taken outside the integral of equation (40) to yield an approximate form given by (ref. 36)

$$\sigma_{\rm em} \approx N_{E1}(E_{\rm GDR}) \int \sigma_{E1}(E)\, dE + N_{E2}(E_{\rm GQR})\, E_{\rm GQR}^2 \int \sigma_{E2}(E)\, \frac{dE}{E^2} \tag{47}$$

where $E_{\rm GDR}$ and $E_{\rm GQR}$ are the energies at the peaks of the giant dipole resonance (GDR) and giant quadrupole resonance (GQR) photonuclear cross sections, respectively. These integrals of photonuclear cross sections over energy are evaluated with the following sum rules:

$$\int \sigma_{E1}(E)\, dE = 60\, \frac{N_P Z_P}{A_P} \tag{48}$$

which is expressed in units of MeV-mb and

$$\int \sigma_{E2}(E) \frac{dE}{E^2} = 0.22\ f Z_P A_P^{2/3} \tag{49}$$

which is expressed in units of μb/MeV. (See ref. 36.)

In equations (48) and (49), N_P is the number of neutrons, Z_P is the number of protons, and A_P is the mass number of the projectile nucleus. The fractional exhaustion of the energy weighted sum rule in equation (49) is (ref. 34)

$$f = \left\{ \begin{array}{ll} 0.9 & (A_P > 100) \\ 0.6 & (40 < A_P \le 100) \\ 0.3 & (40 \le A_P) \end{array} \right\} \tag{50}$$

In equation (47) $E_{\rm GDR}$ and $E_{\rm GQR}$ are the energies at the peaks of the GDR and GQR photonuclear cross sections. For the dipole term it is

$$E_{\rm GDR} = \frac{\hbar c}{2\pi} \left[\frac{m^* c^2 R_0^2}{8J} \left(1 + u - \frac{1 + \varepsilon + 3u}{1 + \varepsilon + u} \varepsilon \right) \right]^{-1/2} \tag{51}$$

which is expressed in units of MeV with

$$u = \frac{3J}{Q'}\ A_P^{-1/3} \tag{52}$$

and

$$R_0 = r_0\, A_P^{1/3} \tag{53}$$

where $\varepsilon = 0.0768$, $Q' = 17$ MeV, $J = 36.8$ MeV, $r_0 = 1.18$ fm, and m^* is 7/10 of the nucleon mass. (See ref. 34.) For the quadrupole term, it is simply given by

$$E_{\rm GQR} = \frac{63}{A_P^{1/3}} \tag{54}$$

which is expressed in units of MeV.

Finally, the single proton or single neutron removal cross sections are obtained from $\sigma_{\rm em}$ (eq. (47)) with proton and neutron branching ratios g_p and g_n, respectively, as

$$\sigma(i) = g_i \sigma_{\rm em} \qquad (i = p \ \text{ or } \ n) \tag{55}$$

The proton branching ratio has been parameterized by Westfall et al. as

$$g_p = \min \left[\frac{Z_P}{A_P}, 1.95\ \exp\left(-0.075 Z_P\right) \right] \tag{56}$$

where Z_P is the number of protons, and the minimum value of the two quantities in square brackets is taken. (See ref. 34.) This parameterization is satisfactory for heavier nuclei ($Z_P > 14$). For light nuclei, however, the following branching ratios are used:

$$g_p = \left\{ \begin{array}{ll} 0.5 & (Z_P < 6) \\ 0.6 & (6 \le Z_P \le 8) \\ 0.7 & (8 < Z_P < 14) \end{array} \right\} \tag{57}$$

For neutrons, the branching ratio is given by

$$g_n = 1 - g_p \tag{58}$$

Database Evaluation

Measurements have been made for carbon ion beams on carbon target at the four energies of 250 A MeV (ref. 38), 600 A MeV (ref. 22), 1.05 A GeV (ref. 39), and 2.1 A GeV (ref. 39) and are shown in figure 2 with results from NUCFRG2. These fragmentation cross sections are among the best known (ref. 40). The effects of the coulomb trajectory are clearly apparent in the energy dependence of the lighter mass fragment cross sections of Li and Be below 100 A MeV. These coulomb effects will be even more important for projectiles and targets with greater charge. Figure 3 shows the NUCFRG2 model at very low energy (11.7 A MeV) for ^{16}O projectiles onto an ^{92}Mo target where coulomb trajectory corrections are very important (ref. 40). The cross sections of the resulting charge removal seem well represented by NUCFRG2 even at such low energies. The addition of exchange poles to the model would bring the cross sections of $\Delta Z = 0$ into agreement, which can be judged by the proton exchange pole contribution for $\Delta Z = -1$ as shown in figure 3. Clearly, the model gives a far better result than expected.

There are three projectile and target combinations for which two groups, 1.55 A GeV (ref. 20) and 1.88 A GeV (ref. 34) have measured cross sections at nearly the same energy. On the basis of NUCFRG2, very small cross section differences are expected at these energies. (See fig. 2.) The cross sections from NUCFRG2 tend to agree more closely with the experiments of Westfall et al. (ref. 34) and are 10 to 50 percent higher than those measured by Cummings et al. (ref. 20) as shown in figures 4 to 6. However, for charges between 10 to 13, NUCFRG2 agrees more closely with the data of Cummings et al.

To better quantify the comparison of results shown in figures 4 to 6, a chi square analysis is used. A comparison of NUCFRG2 model with the experiments of Westfall et al. (ref. 34) and Cummings et al. (ref. 20) is shown in table 1 for iron projectiles on three targets. Shown in table 1 are the total chi square value and the average chi square contribution per degree of freedom n. Clearly, the data for producing Al fragments in the Westfall et al. experiments show large systematic errors and is the dominant contribution to the chi square value. Except for the Al datum, the model shows good agreement with the data of Westfall et al. for carbon and copper

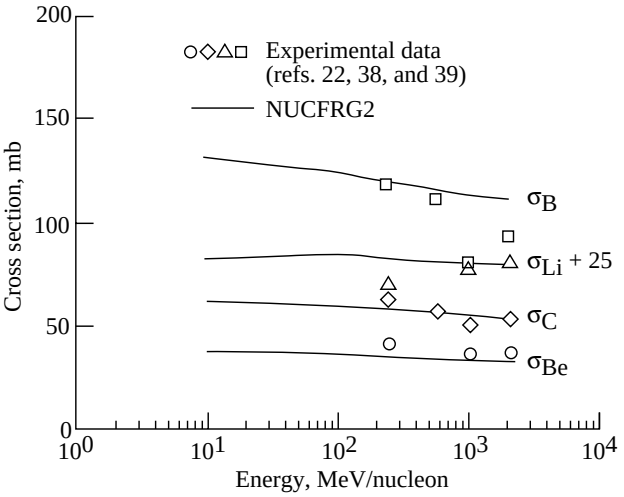

Figure 2. Charge removal cross sections for carbon ions on a carbon target as a function of projectile energy.

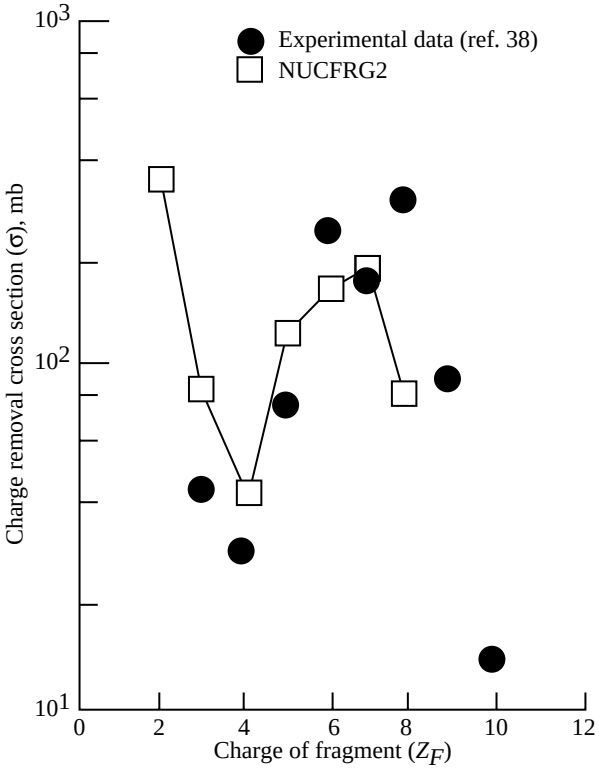

Figure 3. Charge-removal cross sections for 11.7 A MeV ^{16}O projectiles onto ^{92}Mo targets.

targets. The greater discrepancy for the lead targets surely results from simplified nuclear matter distribution in NUCFRG2. A diffuse model instead of the uniform spheres of the NUCFRG2 computation

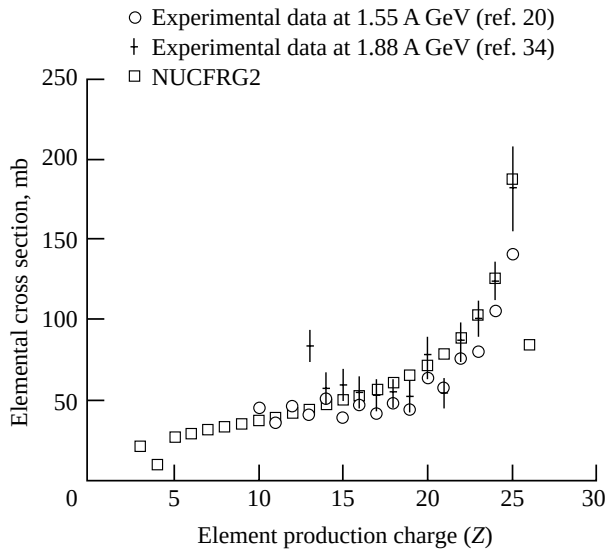

Figure 4. Charge removal cross sections for Fe ions on a carbon target compared with measurements by Westfall et al. and Cummings et al.

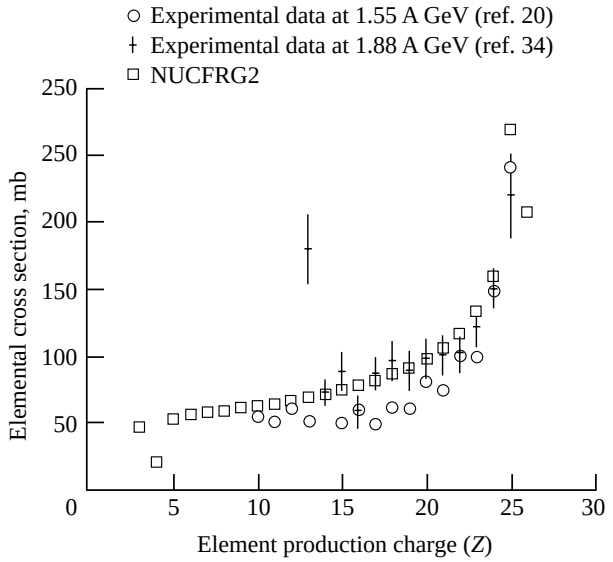

Figure 5. Charge removal cross sections for Fe ions on a copper target compared with measurements by Westfall et al. and Cummings et al.

is recommended. This growing discrepancy with increasing target mass leads to a lack of unitarity given by the condition

$$A_P\,\sigma_{\text{abs}} = \sum\ A_i \sigma_i \qquad (59)$$

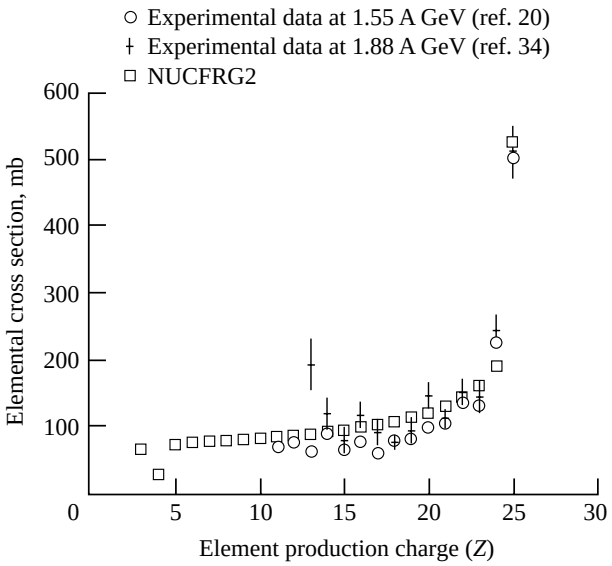

Figure 6. Charge removal cross sections for Fe ions on a lead target compared with measurements by Westfall et al. and Cummings et al.

In generating nuclear data for transport studies, a correction is applied to targets with a charge number greater than 29 to ensure mass conservation. Comparing the NUCFRG2 model with the data of Cummings et al. shows similar trends with target mass, but the overall agreement with the data of Cummings et al. is inferior to agreement with the data of Westfall et al. as we have noted in the discussion of figures 4 to 6.

The chi square analysis has been used to compare how well one experimental group compares with the results of another group. These results are shown in table 2. From table 2, it is clear that the NUCFRG2 model better represents the two sets of experimental data than either experimental data set represents the other. The systematic errors led to a chi square per datum of 10 to 15, which might be used as a measure of goodness of fit of the NUCFRG2 model.

The fragmentation cross section for several projectile species on carbon targets at several energies are shown in table 3 (refs. 19 to 22, 34, 38, and 41). In the table, cross sections for the fragment charge, the mass for isotopic measurements, the statistical uncertainty, the results of NUCFRG2, and the chi square per datum are shown. If the error in the experimental data were only statistical, then a chi square per datum value of 1 to 2 would be appropriate and a data set with near zero would be viewed with suspicion. Clearly, large values of chi square per datum indicate possible systematic errors or errors in the NUCFRG2

model and it is difficult to make a clear judgment in all cases. Although the ^{12}C projectile isotonic breakup cross sections fit the data perhaps too well, the isotopic distributions of NUCFRG2 are distinctly different from the experiments in most cases.

Unlike the ^{12}C projectiles, the isotonic and the isotopic fragmentations of ^{16}O are outside the statistical uncertainty of the experiments. The ^{23}Na and ^{24}Mg fragmentations show a strong even-odd effect on fragment charge, which are not well represented in the results of the NUCFRG2 model. The more massive projectiles of ^{40}Ar and ^{56}Fe are better represented by the NUCFRG2 model for the isotope distributions. The isotonic fragmentation cross sections for ^{56}Fe on carbon targets are represented well by the NUCFRG2 model.

The isotopic distributions of light fragments shown in table 4 are improperly distributed in the breakup of ^{12}C projectiles on numerous targets. In particular, the isotopes of B are produced in disproportionate numbers for all targets. We also note that the cross sections from the NUCFRG2 model for heavier targets are systematically low and probably result from the assumption of uniform spheres in the nucleus (ref. 31). This error is corrected in the model presented herein by applying a renormalization factor N_R to individual fragment cross sections

$$N_R = A_p \, \sigma_{\text{abs}} / \sum_j A_j \, \sigma_j \qquad (60)$$

where p denotes the projectile and j the fragment. This unitarity factor is used in the final database but is not included in tables 1 to 7.

The light fragment distributions through carbon isotopes are examined best by comparing the ^{16}O breakup cross sections. We again suspect significant nuclear structure effects that are not well represented by the Rudstam formalism. Heavier targets show larger differences with the NUCFRG2 model presented herein because of effects of the diffuseness at the nuclear surface. The poor representation of the isotopic distribution of light fragments persists in the ^{42}Ar fragmentation in KCl shown in table 6.

The remaining ^{56}Fe fragmentation data in table 7 are the measurements of Westfall et al. (ref. 34) and Cummings et al. (ref. 20). Generally the NUCFRG2 model agrees with the two experiments (at least to the degree that they agree with each other) except for the few spurious data points in the data of Westfall et al. The model is most accurate for light targets.

The variation of chi square per n over the available experimental data is summarized in table 8. Recall that the estimate of systematic experimental error obtained by comparing the Westfall et al. iron data with that of Cummings et al. gives the experimental chi square per n of 4 to 12. The corresponding model chi square per n for NUCFRG2 for these experimental data sets is from 2 to 7, which shows that NUCFRG2 tends to split the difference between the two experiments. The iron fragmentation for targets below sulfer show comparable model chi square per n between 2.3 and 7.4. The model chi square per n for targets above sulfer indicate systematic model errors, which need to be resolved. Clearly, the current experimental data are adequate as a measure of model improvement. However, current experimental accuracy is inadequate to evaluate the resulting nuclear database to the accuracy required for shield design.

More recently, fragmentation cross sections were measured at the Lawrence Berkeley Laboratory for 600 A MeV iron beams on 2-cm-thick polyethylene $(CH_2)_x$ targets (ref. 41). The results are shown in figure 7. A systematic error was introduced by an electronic trigger inefficiency to fragments lighter than Ne. The chi square per datum for fragments heavier than Ne is 3×10^{-4}, while for the complete data set the chi square per datum is 6×10^{-4}.

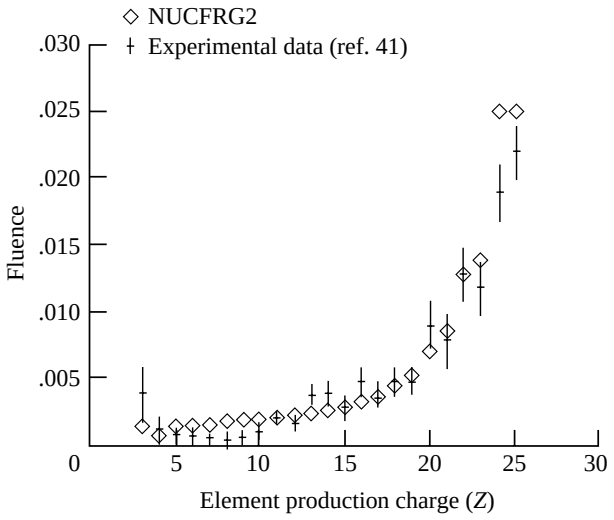

Figure 7. Charge removal cross sections for Fe ions at 600 A MeV in polyethylene.

The comparison of the NUCFRG2 model with the measured fragmentation cross sections mainly tests the dependence of $\sigma(\Delta A)$ and the applicability of the formalism of Rudstam for the charge distribution. A more sensitive test of the model representation of the ablation process is to compare the numbers and the types of particles produced. The multiplicities of the charged reaction products were measured by

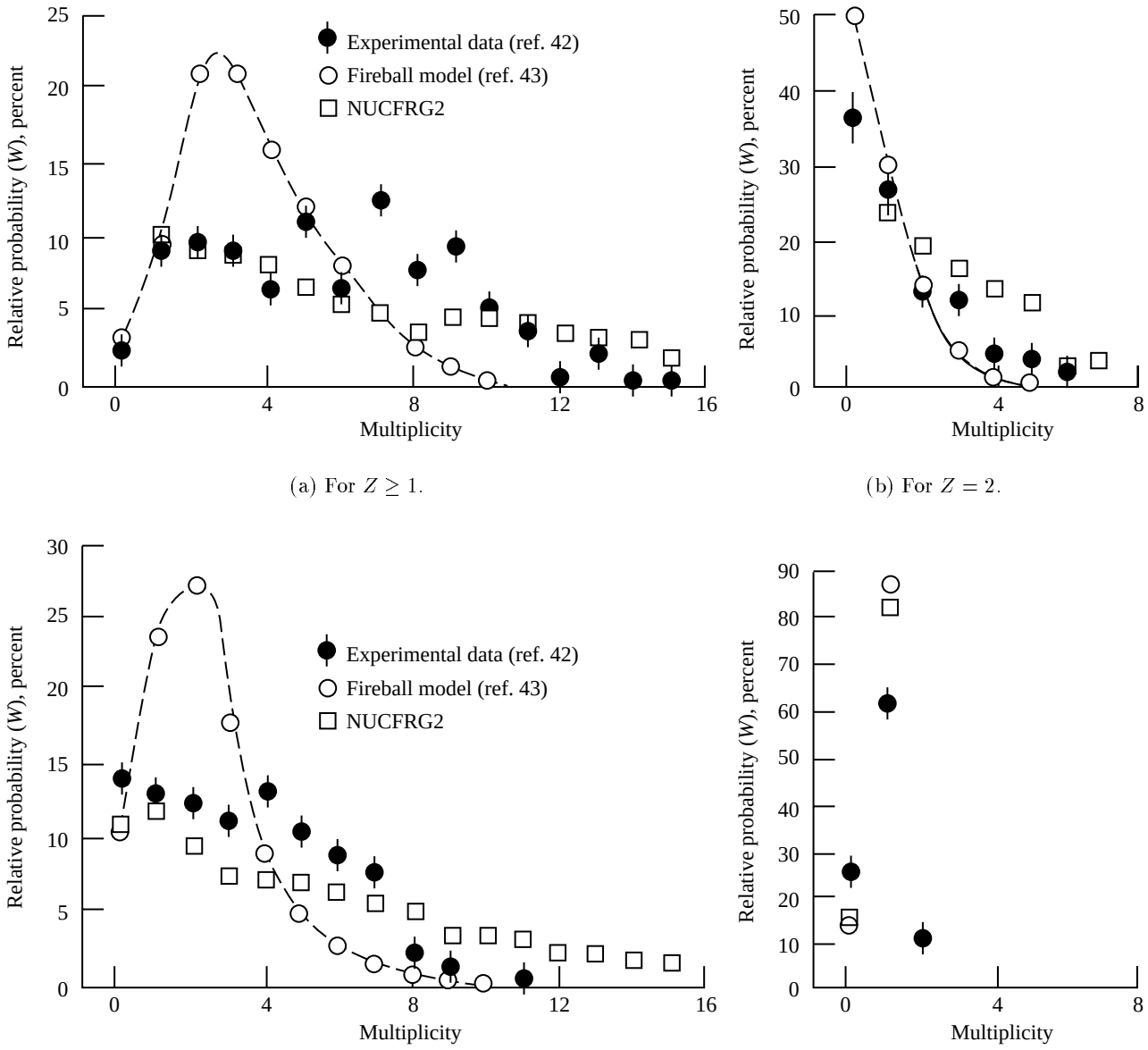

(a) For $Z \geq 1$.

(b) For $Z = 2$.

(c) For $Z = 1$.

(d) For $Z \geq 3$.

Figure 8. Relative probabilities for multiplicity of various charge states for ^{56}Fe ion beams in nuclear emulsion.

Dudkin et al. (ref. 42) and are shown in figure 8 for comparison with calculations with the fireball model (ref. 43) and the version of NUCFRG2 presented herein. The primary difference between the two models is the semiempirical correction to the excitation energy required by the NUCFRG2 model to fit the atmospheric air shower data (ref. 42) and the implementation of the deexcitation process.

As shown by Dudkin et al., the fireball model shows even qualitative differences in the frequency distribution of multiplicities in nuclear emulsion when compared with the experimental results (ref. 42). In general, the fireball model overestimates the events of low multiplicity and correspondingly underestimates the high multiplicity events. The NUCFRG2 model gives a much improved distribution of events, although the predicted number of high multiplicity events appears greater than is seen experimentally. However, the resolution of the multiplicity when many high-energy secondaries are produced at one apex is not good. Clearly, if some of the observed several prong events were in fact of higher multiplicity, then good agreement between the NUCFRG2 model and the experiments is conceivable.

Concluding Remarks

The analysis of experimental data of iron beam interactions in polyethylene and aluminum targets has resulted in an improved semiempirical model for nuclear database generation. However, this analysis is still unable to unambiguously resolve differences between various experimental groups that use the same projectile and target combinations. Further improvements to the basic model have been made as a result of the presented evaluation. These improvements are correcting the charge distributions in the formulation of Rudstam for light nuclei where shell structure effects cause important deviations from simple systematic behavior. Even with these improvements, there is need for improved target mass dependence where the skin diffuseness is suspected to require further correction.

There are two approaches to improve the generation code of the NUCFRG2 nuclear database. The first is incremental improvements to the semiempirical model. The second approach is more radical and involves the further development of quantum based methods. Ultimately, model development is still limited by the systematic errors in the experimental fragmentation data and the paucity of experimental data.

The semiempirical model is first limited by the assumed uniform nuclear matter distribution. This assumption is the main source of nonconservation of mass and charge for massive targets that is temporarily corrected by forcing unitarity; however, a fully correct description must replace the uniform sphere model with realistic nuclear density distributions. Although ad hoc corrections have been made for structure effects in the low mass fragments (mass number less than 10), errors remain in the isotope distributions lighter than Ne. Improved methods for representing the distribution of excitation energy and corrections to Rudstam's distribution will be required. The distribution of mass and charge in the final ablation products depends on the excitation energy. Although the multiplicities are reasonable and are greatly improved over the fireball model, the agreement with atmospheric air shower data might be improved.

The microscopic description of nuclear fragmentation proceeds from a multiple-scattering theory (MST), a description that uses the Glauber or eikonal approximation of the multiple-scattering series, which results from a systematic reduction of relativistic MST or a nonrelativistic MST. A relativistic or nonrelativistic model may be cast as a distorted-wave series by using an average optical potential for elastic transitions.

A very difficult task still remains in treating multiple inelastic transitions that occur in heavy ion fragmentation. The difficulty arises first because of the many irreducible diagrams that contribute to any integral equation that would be formulated. Typically, integral equations of six or more dimensions will occur for inelastic transitions. This occurence of six or more dimensions is in comparison with the 3-dimensional integral equations that appear in the optical model formulation of elastic heavy ion scattering. Also, a perturbative approach becomes difficult because of the large number of terms required for heavy ion scattering and the complexity of summing over intermediate state variables.

A more practical approach is to use the forward scattering assumptions of the eikonal model, which is expected to be valid at high energies. This approach allows for closed-form expressions to be derived for the multistep processes. Here, the eikonal approximation can be applied in both the nonrelativistic MST or a relativistic MST. A relativistic eikonal model could allow the effects of negative-energy states on nuclear fragmentation to be considered. A study of the one- and two-step contributions to fragmentation could be made in the relativistic or nonrelativistic models to provide a test of the validity of the eikonal approximation and the neglecting of off-shell effects. In all of the approaches mentioned, a treatment of meson and antinucleon production in the MST should be considered.

An alternative to the use of an MST or the Glauber model in formulating the fragmentation process is to derive transport equations from an MST. In the MST, it is difficult to include the cascade of projectile knockouts through the projectile prefragments. In nucleon-nucleus scattering, the number of cascade particles is small at low to medium energies that are typical of the relative energy expected between knockouts and prefragments. However, the multiple-scattering cascade terms will depend strongly on the initial trajectory of the knockouts, which will lead to a heavy computational burden. A derivation of the simple final state interaction (FSI) corrections may help to simplify an MST approach. The transport models are a more tractable approach to the cascade problem. These models are usually used to study the knockout spectrum of nucleons. In some cases, the spectrum of residual energies after the cascade is used to predict the final fragment mass yields. The reliance upon classical methods that ignore quantum effects and the use of Monte-Carlo simulations that require large

computational times may limit the usefulness of this approach.

In describing the abrasion-ablation process, the dynamical model of choice should be used to formulate the creation of the prefragment state in an arbitrary configuration. The description of the prefragment configuration requires the variables mass and charge number, the distribution of excitation energies, and the spin to be complete. This description should distinguish whether the creation of the prefragment occured after multistep nucleon removal or cluster removal and predict the correct yields and the energy spectrum of light fragments in the reaction. Such a description would require a large amount of nuclear structure input. For example, the study of cluster abrasion requires a more detailed description of the nuclear ground state than the independent particle model. The development of the formalism for overlap function of the nuclear ground state for competing cluster configurations is required to aid the description of the abrasion process. Clearly, nuclear shell effects will be more correctly described in such a formalism. Much information on the level densities and decay modes of nuclei is well known, although the treatment of extremely high excitation energies is less understood. Also less understood is whether there is a one-to-one correspondence between the decay of excited prefragments produced in heavy ion fragmentation and the equilibrium decay treated by statistical methods. Further studies in these areas should be made.

NASA Langley Research Center
Hampton, VA 23681-0001
July 7, 1995

Appendix

Abrasion Model Formula

Two functions F and P used in the formalism given in the text are described in this appendix. For $r_T > r_P$, where r_T is target radius and r_P is projectile radius, we have

$$P = 0.125(\mu\nu)^{1/2}\left(\frac{1}{\mu} - 2\right)\left(\frac{1-\beta}{\nu}\right)^2 - 0.125\left[0.5(\mu\nu)^{1/2}\left(\frac{1}{\mu} - 2\right) + 1\right]\left(\frac{1-\beta}{\nu}\right)^3 \tag{A1}$$

and

$$F = 0.75(1-\nu)^{1/2}\left(\frac{1-\beta}{\nu}\right)^2 - 0.125[3(1-\nu)^{1/2} - 1]\left(\frac{1-\beta}{\nu}\right)^3 \tag{A2}$$

with

$$\nu = r_P/(r_P + r_T) \tag{A3}$$

$$\beta = b/(r_P + r_T) \tag{A4}$$

and

$$\mu = (1/\nu) - 1 = r_T/r_P \tag{A5}$$

(See ref. 32.) Equations (A1) and (A2) are valid when the collision is peripheral (i.e., the two nuclear volumes do not completely overlap). In this case, the impact separation r is restricted so that

$$r_T - r_P \le r \le r_T + r_P \tag{A6}$$

If the collision is central, then the projectile nucleus volume completely overlaps the target nucleus volume ($r < r_T - r_P$), and all the projectile nucleons are abraded. In this case, equations (A1) and (A2) are replaced by

$$P = -1 \tag{A7}$$

and

$$F = 1 \tag{A8}$$

and there is no ablation of the projectile, because it was destroyed by the abrasion.

For the case where $r_P > r_T$ and the collision is peripheral, equations (A1) and (A2) become

$$P = 0.125(\mu\nu)^{1/2}\left(\frac{1}{\mu} - 2\right)\left(\frac{1-\beta}{\nu}\right)^2 - 0.125\left\{0.5\left(\frac{\nu}{\mu}\right)^{1/2}\left(\frac{1}{\mu} - 2\right) - \left[(1/\nu)(1-\mu^2)^{1/2} - 1\right]\frac{[(2-\mu)\mu]^{1/2}}{\mu^{1/2}}\right\}\left(\frac{1-\beta}{\nu}\right)^3 \tag{A9}$$

and

$$F = 0.75(1-\nu)^{1/2}\left(\frac{1-\beta}{\nu}\right)^2 - 0.125\left\{\frac{3(1-\nu)^{1/2}}{\mu} - \frac{[1-(1-\mu^2)^{3/2}][1-(1-\mu)^2]^{1/2}}{\mu^3}\right\}\left(\frac{1-\beta}{\nu}\right)^3 \tag{A10}$$

where the impact separation is restricted so that

$$r_P - r_T \le r \le r_P + r_T \tag{A11}$$

(See ref. 33.) For a central collision ($r < r_P - r_T$) with $r_P > r_T$, equations (A9) and (A10) become

$$P = \left[\frac{1}{\nu}(1-\mu^2)^{1/2} - 1\right]\left[1 - \left(\frac{\beta}{\nu}\right)^2\right]^{1/2} \tag{A12}$$

and

$$F = \left[1 - (1-\mu^2)^{3/2}\right]\left[1 - \left(\frac{\beta}{\nu}\right)^2\right]^{1/2} \tag{A13}$$

References

1. Wilson, John W.; Thibeault, Sheila A.; Nealy, John E.; Kim, Myung-Hee; and Kiefer, R. L.: Studies in Space Radiation Shield Performance. *Proceedings of the Engineering & Architecture Symposium*, Prairie View A&M Univ., 1993, pp. 169–176.

2. Kim, Myung-Hee Y.; Wilson, John W.; Thibeault, Sheila A.; Nealy, John E.; Badavi, Francis F.; and Kiefer, Richard L.: *Performance Study of Galactic Cosmic Ray Shield Materials*. NASA TP-3473, 1994.

3. Eisenberg, Y.: Interaction of Heavy Primary Cosmic Rays in Lead. *Phys. Rev.*, vol. 96, no. 5, Dec. 1954, pp. 1378–1382.

4. Bowman, J. D.; Swiatecki, W. J.; and Tsang, C. F.: *Abrasion and Ablation of Heavy Ions*. LBL-2908, Univ. of California, July 1973.

5. Wilson, John W.; Townsend, Lawrence W.; and Badavi, F. F.: A Semiempirical Nuclear Fragmentation Model. *Nucl. Instrum. & Methods Phys. Res.*, vol. B18, no. 3, Feb. 1987, pp. 225–231.

6. Wilson, John W.; Townsend, Lawrence W.; and Badavi, Forooz F.: Galactic HZE Propagation Through the Earth's Atmosphere. *Radiat. Res.*, vol. 109, no. 2, Feb. 1987, pp. 173–183.

7. Hüfner, J.; Schäfer, K.; and Schürmann, B.: Abrasion-Ablation in Reactions Between Relativistic Heavy Ions. *Phys. Rev. C*, vol. 12, no. 6, Dec. 1975, pp. 1888–1898.

8. Bleszynski, M.; and Sander, C.: Geometrical Aspects of High-Energy Peripheral Nucleus-Nucleus Collisions. *Nucl. Phys. A*, vol. 326, nos. 2–3, Sept. 1979, pp. 525–535.

9. Townsend, L. W.: Abrasion Cross Section for ^{20}Ne Projectiles at 2.1 GeV/Nucleon. *Canadian J. Phys.*, vol. 61, no. 1, Jan. 1983, pp. 93–98.

10. Cucinotta, Francis A.; and Dubey, Rajendra R.: Alpha-Cluster Description of Excitation Energies in 12C(12C,3α)X at 2.1A GeV. *Phys. Rev. C: Nucl. Phys.*, vol. 50, no. 2, Aug. 1994, pp. 1090–1096.

11. Cucinotta, F. A.; and Dubey, R. R.: Cluster Abrasion of Large Fragments in Relativistic Heavy Ion Fragmentation. *Bull. Am. Phys. Soc.*, vol. 39, no. 5, Oct. 1994, p. 1401.

12. Oliveira, Luiz F.; Donangelo, Raul; and Rasmussen, John O.: Abrasion-Ablation Calculations of Large Fragment Yields From Relativistic Heavy Ion Reactions. *Phys. Rev. C*, vol. 19, no. 3, Mar. 1979, pp. 826–833.

13. Wilson, John W.: Composite Particle Reaction Theory. Ph.D. Diss., College of William and Mary, June 1975.

14. Cucinotta, Francis A.; and Dubey, Rajendra R.: *Final State Interactions and Inclusive Nuclear Collisions*. NASA TP-3353, 1993.

15. Feshbach, Herman; Kerman, Arthur; and Koonin, Steven: The Statistical Theory of Multi-Step Compound and Direct Reactions. *Ann. Phys.*, vol. 125, 1980, pp. 429–476.

16. Griffin, J. J.: Statistical Model of Intermediate Structure. *Phys. Rev. Lett.*, vol. 17, no. 9, Aug. 1966, pp. 478–481.

17. Tamura, T.; Udagawa, T.; and Lenske, H.: Multistep Direct Reaction Analysis of Continuum Spectra in Reactions Induced by Light Ions. *Phys. Rev. C*, vol. 26, no. 2, Aug. 1982, pp. 379–404.

18. Cucinotta, Francis A.: Forward Production of Protons in Relativistic 12C–Nucleus Collisions. *J. Phys. G: Nucl. Part. Phys.*, vol. 20, 1994, pp. 1803–1815.

19. Cucinotta, Francis A.; Townsend, Lawrence W.; and Wilson, John W.: *Description of Alpha-Nucleus Interaction Cross Sections for Cosmic Ray Shielding Studies*. NASA TP-3285, 1993.

20. Cummings, J. R.; Binns, W. R.; Garrard, T. L.; Israel, M. H.; Klarmann, J.; Stone, E. C.; and Waddington, C. J.: Determination of the Cross Sections for the Production of Fragments From Relativistic Nucleus-Nucleus Interactions. I. Measurements. *Phys. Rev. C*, vol. 42, no. 6, Dec. 1990, pp. 2508–2529.

21. Tull, C. E.: *Relativistic Heavy Ion Fragmentation at HISS*. LBL-29718, Univ. of California, Oct. 1990.

22. Webber, W. R.; Kish, J. C.; and Schrier, D. A.: Individual Isotopic Fragmentation Cross Sections of Relativistic Nuclei in Hydrogen, Helium, and Carbon Targets. *Phys. Rev. C: Nucl. Phys.*, vol. 41, no. 2, Feb. 1990, pp. 547–565.

23. Webber, W. R.; Kish, J. C.; and Schrier, D. A.: Individual Charge Changing Fragmentation Cross Sections of Relativistic Nuclei in Hydrogen, Helium, and Carbon Targets. *Phys. Rev. C: Nucl. Phys.*, vol. 41, no. 2, Feb. 1990, pp. 533–546.

24. Shavers, Mark R.; Frankel, Kenneth; Miller, Jack; Schimmerling, Walter; Townsend, Lawrence W.; and Wilson, John W.: The Fragmentation of 670A MeV Neon-20 as a Function of Depth in Water. III. Analytical Multigeneration Transport Theory. *Radiat. Res.*, vol. 136, no. 1, Oct. 1993, pp. 1–14.

25. Shinn, J. L.; Wilson, J. W.; Badavi, F. F.; Benton, E. V.; Csige, I.; Frank, L.; and Benton, E. R.: HZE Beam Transport in Multilayered Materials. *Radiat. Meas.*, vol. 23, no. 1, Jan. 1994, pp. 57–64

26. Badavi, F. F.; Townsend, L. W.; Wilson, J. W.; and Norbury, J. W.: An Algorithm for a Semiempirical Nuclear Fragmentation Model. *Comput. Phys. Commun.*, vol. 47, nos. 2–3, Nov.–Dec. 1987, pp. 281–294.

27. Townsend, Lawrence W.; Wilson, John W.; Tripathi, Ram K.; Norbury, John W.; Badavi, Francis F.; and Khan, Ferdous: *HZEFRG1: An Energy-Dependent Semiempirical Nuclear Fragmentation Model*. NASA TP-3310, 1993.

28. Dymarz, R.; and Kohmura, T.: *The Mean Free Path of Protons in Nuclei and the Nuclear Radius.* Ref: 58/82, Nuclear Physics Lab., Oxford Univ., 1982.

29. Wilson, John W.; Chun, Sang Y.; Badavi, Francis F.; and John, Sarah: *Coulomb Effects in Low-Energy Nuclear Fragmentation*. NASA TP-3352, 1993.

30. Norbury, John W.; Cucinotta, F. A.; Townsend, L. W.; and Badavi, F. F.: Parameterized Cross Sections for Coulomb Dissociation in Heavy-Ion Collisions. *Nucl. Instrum. & Methods Phys. Res.*, vol. B31, no. 4, June 1988, pp. 535–537.

31. Wilson, J. W.; and Townsend, L. W.: An Optical Model for Composite Nuclear Scattering. *Canadian J. Phys.*, vol. 59, no. 11, Nov. 1981, pp. 1569–1576.

32. Gosset, J.; Gutbrod, H. H.; Meyer, W. G.; Poskanzer, A. M.; Sandoval, A.; Stock, R.; and Westfall, G. D.: Central Collisions of Relativistic Heavy Ions. *Phys. Rev. C*, vol. 16, no. 2, Aug. 1977, pp. 629–657.

33. Morrissey, D. J.; Marsh, W. R.; Otto, R. J.; Loveland, W.; and Seaborg, G. T.: Target Residue Mass and Charge Distributions in Relativistic Heavy Ion Reactions. *Phys. Rev. C*, vol. 18, no. 3, Sept. 1978, pp. 1267–1274.

34. Westfall, G. D.; Wilson, Lance W.; Lindstrom, P. J.; Crawford, H. J.; Greiner, D. E.; and Heckman, H. H.: Fragmentation of Relativistic ^{56}Fe. *Phys. Rev. C*, vol. 19, no. 4, Apr. 1979, pp. 1309–1323.

35. Rudstam, G.: Systematics of Spallation Yields. *Zeitschrift fur Naturforschung*, vol. 21a, no. 7, July 1966, pp. 1027–1041.

36. Bertulani, Carlos A.; and Baur, Gerhard: Electromagnetic Processes in Relativistic Heavy Ion Collisions. *Phys. Rep.*, vol. 163, nos. 5 & 6, June 1988, pp. 299–408.

37. Aleixo, A. N. F.; and Bertulani, C. A.: Coulomb Excitation in Intermediate-Energy Collisions. *Nucl. Phys.*, vol. A505, no. 2, Dec. 1989, pp. 448–470.

38. Kidd, J. M.; Lindstrom, P. J.; Crawford, H. J.; and Woods, G.: Fragmentation of Carbon Ions at 250 MeV/Nucleon. *Phys. Rev. C*, vol. 37, no. 6, June 1988, pp. 2613–2623.

39. Olson, D. L.; Berman, B. L.; Greiner, D. E.; Heckman, H. H.; Lindstrom, P. J.; and Crawford, H. J.: Factorization of Fragment-Production Cross Sections in Relativistic Heavy-Ion Collisions. *Phys. Rev. C.*, vol. 28, no. 4, Oct. 1983, pp. 1602–1613.

40. Lefort, Marc: Mass Distribution in Dissipative Reactions—The Frontier Between Fusion and Deep Inelastic Transfers. *Deep-Inelastic and Fusion Reactions With Heavy Ions*, W. von Oertzen, ed., Volume 117 of *Lecture Notes in Physics*, Springer-Verlag, 1980, pp. 25–42.

41. Zeitlin, C. J.; Frankel, K. A.; Gong, W.; Heilbronn, L.; Lampo, E. J.; Leres, R.; Miller, J.; and Schimmerling, W.: A Modular Solid State Detector for Measuring High Energy Heavy Ion Fragmentation Near the Beam Axis. *Radiat. Meas.*, vol. 23, no. 1, Jan. 1994, pp. 65–81.

42. Dudkin, V. E.; Kovalev, E. E.; Nefedov, N. A.; Antonchik, V. A.; Bogdanov, S. D.; Ostroumov, V. I.; Crawford, H. J.; and Benton, E. V.: Multiplicities of Secondaries in Interactions of 1.8 GeV/Nucleon ^{56}Fe Nuclei With Photoemulsion and the Cascade Evaporation Model. *Nucl. Phys.*, vol. A509, no. 4, Mar. 1990, pp. 783–799.

43. Westfall, G. D.; Gosset, J.; Johansen, P. J.; Poskanzer, A. M.; Meyer, W. G.; Gutbrod, H. H.; Sandoval, A.; and Stock, R.: Nuclear Fireball Model for Proton Inclusive Spectra From Relativistic Heavy-Ion Collisions. *Phys. Rev. Lett.*, vol. 37, no. 18, Nov. 1976, pp. 1202–1205.

Table 1. Chi Square Analysis of Iron Fragmentation Model

System	NUCFRG2 and Westfall et al.				NUCFRG2 and Cummings et al.	
	χ^2	χ^2 without Al data	χ^2/n	χ^2/n without Al data	χ^2	χ^2/n
Fe + C	50.2	16.0	5	1.8	48.3	3.7
Fe + Cu	200.6	22.9	20	2.5	78.4	6.0
Fe + Pb	177.4	56.2	18	6.2	83.1	6.7

Table 2. Chi Square Analysis of Iron Fragmentation Experiments

System	Westfall et al. and Cummings et al.				Cummings et al. and Westfall et al.			
	χ^2	χ^2 without Al data	χ^2/n	χ^2/n without Al data	χ^2	χ^2 without Al data	χ^2/n	χ^2/n without Al data
Fe + C	85.6	43.3	8.6	4.8	54.6	33.6	5.5	3.7
Fe + Cu	424.4	108.4	42.4	12.0	160.3	69.4	16.0	7.7
Fe + Pb	348.8	79.5	34.9	8.8	143.1	55.8	14.3	6.2

Table 3. Chi Square Analysis of Fragmentation Cross Sections of Projectile Ions on Carbon Targets

[See page 32 for footnotes]

Projectile	Fragment charge	Fragment mass number	Experiment cross section, mb	Experiment uncertainty, mb	NUCFRG2 cross section, mb	Chi square per degree of freedom (*n*)
^{11}B						
326 A MeV[a]	4		105.9	1.59	99.31	
	3		30.1	.45	56.84	
						6.508
^{12}C						
250 A MeV[b]	6	11	55.97	4.06	56.19	
	6	10	5.33	.81	.37	
	5	11	65.61	2.55	56.33	
	5	10	47.50	2.42	57.46	
	4	10	5.88	9.70	3.47	
	4	9	10.44	.85	14.21	
	4	7	22.64	1.49	20.37	
	3	8	1.33	1.00	.11	
	3	7	17.19	3.00	20.07	
	3	6	26.35	2.10	30.80	
						8.504
^{12}C						
403 A MeV[a]	5		106.0	1.59	114.62	
	4		29.6	.89	40.79	
						.929
^{12}C						
418 A MeV[a]	5		111.2	1.67	114.50	
	4		32.1	.96	40.66	
						.949
^{12}C						
561 A MeV[a]	5		108.7	1.63	113.07	
	4		30.3	.91	40.16	
						1.295
^{12}C						
600 A MeV[c]	6	11	53.6	.80	54.1	
	6	10	2.1	.11	.3	
	5	11	70.7	1.06	54.3	
	5	10	38.6	.58	55.3	
	4	10	5.6	.28	3.3	
	4	9	9.6	.29	13.52	
	4	7	15.5	.47	19.53	
						3.092
^{12}C						
693 A MeV[a]	5		110.1	1.65	112.41	
	4		34.9	1.05	39.76	
						0.321

Table 3. Continued

Projectile	Fragment charge	Fragment mass number	Experiment cross section, mb	Experiment uncertainty, mb	NUCFRG2 cross section, mb	Chi square per degree of freedom (*n*)
^{12}C						
915 A MeV[a]	5		109.4	1.64	111.1	
	4		33.6	1.01	39.0	
						0.387
^{12}C						
1016 A MeV[a]	5		113.2	1.70	110.8	
	4		36.8	1.10	39.0	
						.072
^{12}C						
1050 A MeV[d]	6	11	44.70	2.80	52.7	
	6	10	4.44	.24	.4	
	5	11	48.60	2.40	52.9	
	5	10	27.90	2.20	54.4	
	4	10	5.34	.29	3.2	
	4	9	10.70	.50	13.1	
	4	7	18.60	.90	19.0	
	3	8	2.40	.18	.1	
	3	7	21.50	1.10	20.5	
	3	6	27.10	2.20	28.5	
	2	6	1.83	.19	.4	
						10.836
^{12}C						
1572 A MeV[a]	5		103.9	1.56	109.2	
	4		35.6	1.07	38.1	
						.211
^{12}C						
2100 A MeV[d]	6	11	46.50	2.30	51.3	
	6	10	4.11	.22	.3	
	5	11	53.80	2.70	51.6	
	5	10	35.10	3.40	53.7	
	4	10	5.81	.29	3.2	
	4	9	10.63	.53	12.7	
	4	7	18.61	.93	18.5	
	3	8	2.18	.15	.1	
	3	7	21.50	1.10	20.0	
	3	6	30.00	2.40	27.9	
	2	6	2.21	.22	.4	
						9.456
^{14}N						
516 A MeV[a]	6		169.2	2.54	124.0	
	5		63.1	1.89	85.8	
	4		27.9	.84	33.8	
						7.828

Table 3. Continued

Projectile	Fragment charge	Fragment mass number	Experiment cross section, mb	Experiment uncertainty, mb	NUCFRG2 cross section, mb	Chi square per degree of freedom (n)
^{16}O						
441 A MeV[a]	7		162.9	2.44	133.8	
	6		160.2	2.40	111.3	
	5		60.7	1.82	75.7	
	4		13.6	.65	32.9	
						9.718
^{16}O						
491 A MeV[a]	7		146.4	2.20	133.3	
	6		146.2	2.19	110.6	
	5		54.7	1.64	75.5	
	4		13.4	.67	32.8	
						7.491
^{16}O						
669 A MeV[a]	7		158.5	2.38	131.7	
	6		159.6	2.39	109.3	
	5		56.5	1.69	74.7	
	4		17.3	.87	32.3	
						10.661
^{16}O						
903 A MeV[a]	7		154.4	2.32	130.4	
	6		152.9	2.29	108.2	
	5		52.4	1.57	73.9	
	4		20.3	1.02	32.1	
						8.331
^{16}O						
1563 A MeV[a]	7		125.3	1.88	128.4	
	6		123.2	1.85	106.1	
	5		46.6	1.40	72.8	
	4		18.2	.91	31.7	
						4.500
^{16}O						
2100 A MeV[d]	8	15	42.90	2.30	57.6	
	8	14	1.67	.12	.6	
	7	15	54.20	2.90	58.0	
	7	14	41.80	3.30	61.7	
	7	13	8.06	.42	6.9	
	7	12	.73	.07	.3	
	6	14	4.71	.31	10.8	
	6	13	27.70	1.40	47.7	
	6	12	65.10	5.20	40.3	
	6	11	18.46	.92	6.0	
	6	10	2.51	.16	.2	
	5	13	.44	.05	.4	
	5	12	2.44	2.15	4.3	
	5	11	26.0	1.30	32.7	

Table 3. Continued

Projectile	Fragment charge	Fragment mass number	Experiment cross section, mb	Experiment uncertainty, mb	NUCFRG2 cross section, mb	Chi square per degree of freedom (*n*)
^{16}O						
2100 A MeV[d]	5	10	20.3	1.60	32.3	
	4	11	.19	.03	.17	
	4	10	3.9	.30	1.9	
	4	9	9.0	.51	9.8	
	4	7	22.3	1.10	16.5	
	3	8	2.5	.18	.09	
	3	7	26.3	1.30	17.9	
	3	6	35.9	2.90	26.2	
	2	6	2.0	.21	.3	
						8.018
^{20}Ne						
468 A MeV[a]	9		106.3	1.60	129.9	
	8		181.0	2.72	136.0	
	7		134.5	4.04	103.5	
	6		135.1	4.05	85.9	
	5		53.7	2.69	70.9	
						12.132
^{20}Ne						
599 A MeV[a]	9		91.6	.14	128.8	
	8		150.6	2.26	134.7	
	7		111.1	3.33	102.6	
	6		125.9	3.78	85.2	
	5		52.6	2.63	72.2	
						7.607
^{20}Ne						
608 A MeV[a]	9		96.9	1.45	128.7	
	8		159.5	2.39	134.6	
	7		118.8	3.56	102.4	
	6		120.2	3.61	85.2	
	5		53.6	2.68	70.2	
						6.655
^{20}Ne						
1057 A MeV[a]	9		87.6	1.31	126.2	
	8		140.1	2.10	132.1	
	7		103.0	3.09	100.7	
	6		119.8	3.59	83.7	
	5		57.2	2.86	69.3	
						6.003
^{23}Na						
461 A MeV[a]	10		132.3	1.98	179.7	
	9		62.1	1.86	118.0	
	8		106.1	3.18	94.1	
	7		89.3	2.68	79.8	
	6		101.2	3.04	70.5	
						11.007

Table 3. Continued

Projectile	Fragment charge	Fragment mass number	Experiment cross section, mb	Experiment uncertainty, mb	NUCFRG2 cross section, mb	Chi square per degree of freedom (*n*)
^{24}Mg						
309 A MeV[a]	11		147.8	2.22	112.2	
	10		133.0	2.00	147.0	
	9		58.1	1.74	109.3	
	8		136.6	2.05	89.8	
	7		89.3	2.68	77.6	
	6		114.3	3.43	69.1	
	5		39.8	1.99	59.0	
						14.072
^{24}Mg						
481 A MeV[a]	11		124.3	1.86	110.5	
	10		111.0	1.67	139.5	
	9		56.3	1.69	107.2	
	8		119.7	1.80	88.5	
	7		89.4	2.68	76.5	
	6		120.4	3.61	68.4	
	5		48.1	2.41	58.3	
						12.297
^{24}Mg						
739 A MeV[a]	11		116.1	1.74	108.7	
	10		102.2	1.53	137.3	
	9		48.7	1.46	105.8	
	8		103.5	1.55	87.2	
	7		75.9	2.28	75.7	
	6		108.6	3.26	67.6	
	5		45.6	4.56	58.0	
						10.124
^{24}Mg						
1455 A MeV[a]	11		116.4	1.75	106.6	
	10		101.5	1.52	134.0	
	9		48.0	1.44	103.8	
	8		106.5	1.60	85.7	
	7		73.8	2.21	74.4	
	6		106.6	3.20	66.8	
	5		48.6	2.43	57.6	
						9.857
^{27}Al						
582 A MeV[a]	12		182.1	2.73	163.7	
	11		95.6	1.43	123.5	
	10		89.4	1.34	97.7	
	9		37.6	1.88	82.8	
	8		81.5	2.44	72.8	
	7		60.2	1.81	65.3	
	6		74.1	3.71	59.3	

Table 3. Continued

Projectile	Fragment charge	Fragment mass number	Experiment cross section, mb	Experiment uncertainty, mb	NUCFRG2 cross section, mb	Chi square per degree of freedom (n)
^{27}Al						
582 A MeV[a]	5		37.6	3.76	51.5	
						5.330
^{40}Ar						
600 A MeV[c]	18	39	146.4	2.20	63.7	
	18	38	72.3	1.08	68.8	
	18	37	8.4	.43	29.7	
	17	39	39.1	.59	63.7	
	17	38	34.9	.52	9.5	
	17	37	59.3	.89	35.9	
	17	36	38.0	.57	49.1	
	17	35	12.3	.61	28.2	
	16	38	.8	.08	.1	
	16	37	5.1	.26	1.2	
	16	36	19.3	.58	4.6	
	16	35	32.6	.49	22.6	
	16	34	51.0	.77	39.8	
	16	33	15.3	.46	28.0	
	16	32	1.1	.11	5.8	
	15	35	1.2	.12	.6	
	15	34	6.3	.32	2.7	
	15	33	23.8	.36	14.7	
	15	32	35.9	1.80	33.4	
	15	31	24.0	1.20	27.9	
	15	30	2.2	.22	6.9	
	14	32	4.1	.21	1.7	
	14	31	17.6	.53	9.6	
	14	30	40.1	.60	28.2	
	14	29	27.6	.41	27.6	
	14	28	9.2	.46	8.3	
	13	30	1.2	.12	1.1	
	13	29	11.8	.35	6.2	
	13	28	20.5	1.03	23.9	
	13	27	33.1	.50	26.6	
	13	26	4.2	.42	10.0	
	12	27	4.1	.21	3.9	
	12	26	23.0	.35	20.0	
	12	25	23.1	.35	25.7	
	12	24	12.7	.38	11.5	
	12	23	1.0	.10	1.2	
						9.591
^{40}Ar						
1650 A MeV[e]	17	39	79.50	19.50	61.89	
	17	38	8.10	4.05	9.33	
	17	37	27.00	8.85	34.92	

Table 3. Continued

Projectile	Fragment charge	Fragment mass number	Experiment cross section, mb	Experiment uncertainty, mb	NUCFRG2 cross section, mb	Chi square per degree of freedom (*n*)
^{40}Ar						
1650 A MeV[e]	17	36	49.50	16.60	47.71	
	17	35	51.00	19.50	27.34	
	17	34	12.00	6.45	4.93	
	16	38	4.35	1.50	.15	
	16	37	11.70	2.70	1.19	
	16	36	12.40	3.00	4.48	
	16	35	24.00	5.40	21.83	
	16	34	49.50	10.80	38.49	
	16	33	31.50	7.05	27.31	
	16	32	10.60	3.00	5.74	
	16	31	.54	.42	.99	
	15	36	.615	.195	.06	
	15	35	2.10	.33	.58	
	15	34	5.85	.825	2.67	
	15	33	18.00	1.80	14.36	
	15	32	27.00	2.70	32.65	
	15	31	21.00	2.10	27.26	
	15	30	3.90	.63	6.83	
	15	29	.315	.195	1.05	
	14	34	.01	.07	.02	
	14	33	1.32	.24	.30	
	14	32	3.00	.24	1.71	
	14	31	11.00	1.80	9.40	
	14	30	37.50	3.15	27.76	
	14	29	25.50	3.00	26.96	
	14	28	13.00	1.95	8.17	
	14	27	.69	.285	1.11	
	13	32	.129	.111	.01	
	13	31	.705	.21	.15	
	13	30	3.00	.405	1.10	
	13	29	10.40	2.25	6.08	
	13	28	19.50	2.40	23.48	
	13	27	25.50	2.85	26.25	
	13	26	7.20	1.28	9.85	
	13	25	.315	.165	1.17	
	12	30	.165	.126	.01	
	12	29	.66	.21	.01	
	12	28	2.10	.495	.71	
	12	27	6.75	1.02	3.86	
	12	26	24.00	2.85	19.77	
	12	25	22.50	3.45	25.33	
	12	24	14.20	1.80	11.46	
	12	23	.96	.315	1.25	
	11	27	.36	.135	.03	

Table 3. Continued

Projectile	Fragment charge	Fragment mass number	Experiment cross section, mb	Experiment uncertainty, mb	NUCFRG2 cross section, mb	Chi square per degree of freedom (*n*)
^{40}Ar						
1650 A MeV[c]	11	26	2.40	0.51	0.45	
	11	25	7.90	1.05	2.42	
	11	24	12.60	2.10	15.91	
	11	23	22.50	3.15	24.49	
	11	22	8.25	1.65	13.13	
	11	21	.255	.123	1.38	
	10	25	.21	.146	.02	
	10	24	1.80	.45	.27	
	10	23	4.80	.54	1.53	
	10	22	12.30	2.25	12.49	
	10	21	16.50	2.55	22.93	
	10	20	8.55	1.80	14.72	
	10	19	.705	.36	1.61	
	9	22	.765	.285	.15	
	9	21	4.35	.81	.98	
	9	20	7.20	1.95	9.46	
	9	19	11.70	2.25	21.69	
	9	18	5.40	1.32	15.93	
	9	17	.345	.315	1.88	
	8	20	.33	.088	.09	
	8	19	3.60	.645	.64	
	8	18	6.75	1.44	6.81	
	8	17	9.75	2.40	20.31	
	8	16	14.20	3.45	16.71	
	8	15	1.23	.615	2.18	
	8	14	.086	.111	.16	
	7	18	.60	.24	.04	
	7	17	2.25	.57	.41	
	7	16	4.65	1.30	4.65	
	7	15	18.00	5.10	18.79	
	7	14	8.70	2.70	17.23	
	7	13	.75	.48	2.52	
	6	16	.375	.165	.02	
	6	15	1.17	.675	.25	
	6	14	4.35	1.50	3.03	
	6	13	10.00	3.00	17.25	
	6	12	10.20	3.30	17.45	
	6	11	1.215	.555	2.88	
	6	10	.18	.24	.11	
	5	13	1.455	.555	.14	
	5	12	2.25	.855	1.86	
	5	11	7.80	2.70	15.64	
	5	10	4.05	1.485	17.18	
	5	9	.495	.27	1.29	

Table 3. Continued

Projectile	Fragment charge	Fragment mass number	Experiment cross section, mb	Experiment uncertainty, mb	NUCFRG2 cross section, mb	Chi square per degree of freedom (*n*)
^{40}Ar						
1650 A MeV[c]	5	8	0.21	0.255	0.01	
						5.313
^{56}Fe						
330 A MeV[a]	25		244.3	7.33	196.8	
	24		182.7	5.48	132.3	
	23		121.1	3.63	107.7	
	22		110.7	3.32	92.2	
	21		89.2	2.68	81.4	
	20		79.6	2.39	73.4	
	19		51.6	2.58	67.2	
	18		44.4	2.22	62.0	
	17		38.2	1.91	57.5	
	16		42.4	2.12	53.5	
						5.471
^{56}Fe						
434 A MeV[a]	25		223.8	3.36	194.8	
	24		175.1	2.63	131.2	
	23		116.1	3.48	106.7	
	22		116.0	3.48	91.4	
	21		79.8	2.39	80.8	
	20		73.9	2.22	73.0	
	19		52.3	2.62	66.8	
	18		48.2	2.41	61.7	
	17		39.5	1.98	57.3	
	16		44.3	2.22	53.4	
	15		24.89	2.49	49.9	
	14		45.7	4.57	47.0	
						4.355
^{56}Fe						
520 A MeV[a]	25		206.2	3.09	193.6	
	24		163.4	2.45	130.2	
	23		115.2	3.46	105.9	
	22		112.3	3.37	91.2	
	21		76.7	2.30	80.4	
	20		71.3	2.14	72.7	
	19		51.8	2.59	66.7	
	18		52.8	2.64	61.5	
	17		40.6	2.03	57.3	
	16		41.7	2.09	53.3	
	15		29.5	1.48	49.9	
	14		48.6	4.86	46.9	
						2.960

Table 3. Continued

Projectile	Fragment charge	Fragment mass number	Experiment cross section, mb	Experiment uncertainty, mb	NUCFRG2 cross section, mb	Chi square per degree of freedom (*n*)
^{56}Fe						
600 A MeV[c]	26	55	164.3	2.46	67.1	
	26	54	28.2	.85	14.7	
	26	53	3.0	.30	3.3	
	25	55	53.7	.81	64.3	
	25	54	66.9	1.00	64.3	
	25	53	64.0	.96	45.5	
	25	52	21.6	.65	14.5	
	25	51	3.9	.39	3.3	
	24	54	4.7	.24	6.6	
	24	53	16.0	.48	20.5	
	24	52	63.6	.95	42.3	
	24	51	60.7	.91	39.5	
	24	50	30.5	.46	16.2	
	24	49	5.1	.15	3.6	
	23	52	1.1	.11	3.4	
	23	51	8.3	.25	11.3	
	23	50	33.1	.50	30.8	
	23	49	43.0	.65	35.7	
	23	48	24.7	.37	18.4	
	23	47	4.9	.49	4.0	
	22	50	1.6	.16	1.9	
	22	49	8.4	.25	6.5	
	22	48	30.5	.46	22.6	
	22	47	40.6	.61	32.0	
	22	46	23.3	.35	20.3	
	22	45	4.0	.40	5.0	
	22	44	.6	.60	1.2	
	21	48	.3	.30	1.1	
	21	47	2.7	.27	3.9	
	21	46	12.8	.38	16.1	
	21	45	28.3	.42	28.7	
	21	44	21.5	.32	22.0	
	21	43	6.9	.34	6.3	
	20	45	2.7	.27	2.6	
	20	44	10.6	.32	11.2	
	20	43	22.6	.34	25.0	
	20	42	22.0	.33	23.0	
	20	41	10.9	.55	7.9	
	20	40	1.3	.13	1.6	
	19	44	.7	.07	.4	
	19	43	2.8	.28	1.8	
	19	42	8.1	.08	7.5	
	19	41	16.6	.50	21.5	
	19	40	14.6	.43	23.2	

Table 3. Continued

Projectile	Fragment charge	Fragment mass number	Experiment cross section, mb	Experiment uncertainty, mb	NUCFRG2 cross section, mb	Chi square per degree of freedom (*n*)
^{56}Fe						
600 A MeV[c]	19	39	7.3	0.37	9.8	
	19	38	1.0	.10	1.8	
	18	41	1.7	.17	1.2	
	18	40	8.0	.40	4.9	
	18	39	17.9	.54	17.8	
	18	38	19.1	.57	22.7	
	18	37	6.1	.31	11.8	
	18	36	1.1	.11	2.1	
	17	39	.9	.09	.8	
	17	38	3.4	.34	3.1	
	17	37	12.5	.38	14.3	
	17	36	13.5	.41	22.0	
	17	35	9.6	.48	13.6	
	17	34	.9	.09	2.6	
	16	37	.6	.06	.5	
	16	36	2.2	.22	2.1	
	16	35	8.0	.40	10.8	
	16	34	14.6	.44	20.5	
	16	33	11.1	.33	15.1	
	16	32	5.6	.28	3.3	
	16	31	1.6	.16	.6	
						3.751
^{56}Fe						
662 A MeV[a]	25		191.6	2.87	192.3	
	24		163.2	2.45	129.2	
	23		114.3	3.43	105.3	
	22		105.3	3.16	90.3	
	21		68.9	2.07	80.0	
	20		69.6	2.09	72.3	
	19		49.8	2.49	66.3	
	18		52.9	5.29	61.5	
	17		41.8	2.09	57.1	
	16		45.8	2.29	53.3	
	15		32.0	3.20	49.8	
	14		48.3	4.83	46.9	
						2.562
^{56}Fe						
724 A MeV[a]	25		166.5	1.75	191.9	
	24		130.9	1.96	128.5	
	23		91.5	2.75	105.1	
	22		87.7	2.63	90.1	
	21		66.1	1.98	79.7	
	20		62.0	1.86	72.3	
	19		45.4	2.27	66.3	

Table 3. Continued

Projectile	Fragment charge	Fragment mass number	Experiment cross section, mb	Experiment uncertainty, mb	NUCFRG2 cross section, mb	Chi square per degree of freedom (*n*)
^{56}Fe						
724 A MeV[a]	18		47.8	2.39	61.3	
	17		35.5	1.78	57.0	
	16		39.6	1.98	53.3	
	15		29.3	2.93	49.8	
	14		44.3	4.43	46.9	
						3.243
^{56}Fe						
944 A MeV[a]	25		177.8	2.67	190.2	
	24		130.4	1.96	127.8	
	23		86.7	2.61	104.2	
	22		85.3	2.56	89.6	
	21		66.7	2.00	79.2	
	20		60.2	1.81	71.9	
	19		41.4	2.07	66.0	
	18		43.4	2.17	61.1	
	17		37.6	1.88	56.9	
	16		43.9	2.19	53.1	
	15		29.8	2.98	49.9	
	14		43.7	4.37	46.7	
						3.231
^{56}Fe						
1086A MeV[a]	25		157.7	2.37	189.3	
	24		113.3	1.70	127.3	
	23		77.9	2.34	103.8	
	22		76.4	2.29	89.3	
	21		56.4	1.69	79.1	
	20		57.8	1.73	71.8	
	19		40.7	2.04	65.8	
	18		42.1	2.10	61.1	
	17		35.4	1.77	56.8	
	16		40.6	2.03	53.1	
	15		28.5	2.85	49.9	
	14		44.1	4.41	46.6	
	13		27.2	2.72	44.0	
	12		35.9	3.57	41.7	
						4.831
^{56}Fe						
1409A MeV[a]	25		162.2	2.43	188.1	
	24		106.8	1.60	126.3	
	23		73.5	2.21	103.0	
	22		72.7	2.18	88.8	
	21		53.3	1.60	78.7	
	20		56.9	1.71	71.6	
	19		40.8	2.04	65.6	

Table 3. Continued

Projectile	Fragment charge	Fragment mass number	Experiment cross section, mb	Experiment uncertainty, mb	NUCFRG2 cross section, mb	Chi square per degree of freedom (*n*)
^{56}Fe						
1409A MeV[a]	18		40.3	2.02	60.8	
	17		35.7	1.79	56.8	
	16		42.3	2.11	53.1	
	15		34.6	3.46	49.8	
	14		42.3	4.23	46.7	
	13		28.4	2.84	44.0	
	12		33.6	3.36	41.7	
						4.851
^{56}Fe						
1512 A MeV[a]	25		160.2	2.40	187.7	
	24		102.4	1.54	125.9	
	23		79.5	2.39	103.0	
	22		79.3	2.38	88.7	
	21		57.1	1.71	78.6	
	20		55.7	1.67	71.5	
	19		41.3	2.07	65.5	
	18		39.5	1.98	60.9	
	17		33.6	1.68	56.7	
	16		39.7	1.99	53.0	
	15		31.1	3.11	49.8	
	14		40.9	4.09	46.6	
	13		28.5	2.85	44.1	
	12		34.2	3.42	41.6	
						4.871
^{56}Fe						
1570 A MeV[f]	25		140.73	3.36	187.7	
	24		105.33	2.69	126.0	
	23		79.32	2.31	102.8	
	22		75.17	2.23	88.5	
	21		57.29	1.92	78.6	
	20		63.37	2.01	71.3	
	19		43.62	1.64	65.7	
	18		47.65	1.72	60.7	
	17		41.45	1.59	56.7	
	16		46.47	1.68	53.0	
	15		39.45	1.53	49.8	
	14		50.99	1.75	46.8	
	13		41.23	1.55	44.0	
	12		45.45	1.62	41.6	
	11		35.83	1.42	39.4	
	10		44.79	1.59	37.0	
						3.094

Table 3. Concluded

Projectile	Fragment charge	Fragment mass number	Experiment cross section, mb	Experiment uncertainty, mb	NUCFRG2 cross section, mb	Chi square per degree of freedom (n)
^{56}Fe						
1615 A MeV[a]	25		150.6	2.26	187.5	
	24		99.7	1.50	125.9	
	23		74.7	2.24	102.7	
	22		73.7	2.21	88.5	
	21		54.5	1.64	78.5	
	20		54.8	1.64	71.5	
	19		38.4	1.92	65.6	
	18		38.6	1.93	60.6	
	17		33.7	1.69	56.8	
	16		36.0	1.80	53.1	
	15		28.1	2.81	49.7	
	14		38.3	3.83	46.8	
	13		25.7	2.57	44.0	
	12		28.9	2.87	41.6	
						6.499
^{56}Fe						
1880 A MeV[g]	25		181.0	27.0	186.8	
	24		124.0	13.0	125.3	
	23		100.0	11.0	102.5	
	22		87.0	11.0	88.3	
	21		54.0	9.0	78.3	
	20		78.0	11.0	71.2	
	19		52.0	7.0	65.5	
	18		55.0	9.0	60.7	
	17		53.0	7.0	56.7	
	16		54.0	10.0	53.0	
	15		59.0	10.0	49.7	
	14		57.0	10.0	46.9	
	13		83.0	11.0	44.1	
						3.864

[a]From reference 23.
[b]From reference 36.
[c]From reference 22.
[d]From reference 39.
[e]From reference 21.
[f]From reference 20.
[g]From reference 34.

Table 4. Chi Square Analysis of Fragmentation Cross Sections of Carbon Projectile Ions on Targets Other Than Carbon

[See page 36 for footnote]

Target	Fragment charge	Fragment mass number	Experiment cross section, mb	Experiment uncertainty, mb	NUCFRG2 cross section, mb	Chi square per degree of freedom (n)
^{9}Be						
1050 A MeV[a]	6	11	44.70	2.60	52.88	
	6	10	4.02	.23	.35	
	5	11	50.70	3.20	52.99	
	5	10	28.80	2.30	55.01	
	4	10	5.08	.39	3.32	
	4	9	11.60	.76	13.14	
	4	7	17.80	.90	19.03	
	3	9	.75	.08	.03	
	3	8	2.36	.14	.10	
	3	7	23.40	1.20	20.61	
	3	6	24.80	2.00	29.03	
	2	6	2.09	.17	.37	
						10.026
^{9}Be						
2100 A MeV[a]	6	11	46.70	2.30	51.51	
	6	10	4.20	.21	.34	
	5	11	53.20	2.90	51.64	
	5	10	31.10	2.60	53.81	
	4	10	5.97	.31	3.25	
	4	9	10.98	.55	12.85	
	4	7	18.91	.95	18.66	
	3	9	.92	.08	.03	
	3	8	2.52	.16	.10	
	3	7	22.80	1.10	20.23	
	3	6	33.10	2.70	28.37	
	2	6	2.54	.25	.36	
						11.964
^{27}Al						
1050 A MeV[a]	6	11	57.80	3.90	59.27	
	6	10	5.06	.37	.38	
	5	11	64.50	5.30	60.09	
	5	10	30.40	3.50	59.66	
	4	10	6.49	.48	3.60	
	4	9	13.90	.90	14.34	
	4	7	19.90	1.10	20.80	
	3	9	.82	.16	.04	
	3	8	2.87	.27	.11	
	3	7	28.50	1.40	22.53	
	3	6	24.90	2.90	31.62	
	2	6	2.00	.29	.40	
						13.464

Table 4. Continued

Target	Fragment charge	Fragment mass number	Experiment cross section, mb	Experiment uncertainty, mb	NUCFRG2 cross section, mb	Chi square per degree of freedom (*n*)
^{27}Al						
2100 A MeV[a]	6	11	59.50	3.10	58.69	
	6	10	4.99	.34	.37	
	5	11	65.20	4.80	59.84	
	5	10	36.40	4.80	58.27	
	4	10	7.02	.40	3.52	
	4	9	12.74	.71	14.02	
	4	7	25.80	1.30	20.43	
	3	9	.88	.12	.04	
	3	8	2.79	.23	.11	
	3	7	27.30	1.40	22.14	
	3	6	36.30	2.90	30.64	
	2	6	2.82	.27	.39	
						13.846
^{63}Cu						
1050 A MeV[a]	6	11	78.10	8.10	70.91	
	6	10	7.53	.70	.43	
	5	11	80.10	7.90	73.88	
	5	10	36.40	9.90	67.08	
	4	10	7.69	.61	4.05	
	4	9	14.30	1.20	16.29	
	4	7	25.00	1.90	23.08	
	3	9	1.05	.38	.04	
	3	8	3.99	.70	.12	
	3	7	32.60	1.90	25.00	
	3	6	33.10	6.00	35.91	
	2	6	3.01	.68	.46	
						23.774
^{63}Cu						
2100 A MeV[a]	6	11	81.40	6.30	72.59	
	6	10	5.38	.55	.42	
	5	11	84.40	9.00	77.16	
	5	10	43.70	9.80	66.28	
	4	10	8.57	.70	4.00	
	4	9	16.10	1.30	15.88	
	4	7	33.70	2.30	22.85	
	3	9	1.38	.36	.04	
	3	8	3.89	.47	.12	
	3	7	31.90	2.30	24.75	
	3	6	47.30	4.50	35.30	
	2	6	3.21	.47	.45	
						23.436

Table 4. Continued

Target	Fragment charge	Fragment mass number	Experiment cross section, mb	Experiment uncertainty, mb	NUCFRG2 cross section, mb	Chi square per degree of freedom (n)
^{107}Ag						
1050 A MeV[a]	6	11	98.00	13.00	83.18	
	6	10	7.70	1.00	.47	
	5	11	110.00	15.00	89.42	
	5	10	43.00	12.00	74.01	
	4	10	8.40	1.20	4.47	
	4	9	23.70	2.70	17.35	
	4	7	21.60	2.70	25.05	
	3	9	1.15	.49	.04	
	3	8	2.80	1.20	.14	
	3	7	42.10	3.40	27.14	
	3	6	38.10	7.60	38.30	
	2	6	3.60	1.40	.49	
						19.443
^{107}Ag						
2100 A MeV[a]	6	11	101.90	9.60	89.88	
	6	10	7.03	.88	.47	
	5	11	109.00	13.00	100.17	
	5	10	65.00	17.00	73.03	
	4	10	8.81	.91	4.41	
	4	9	18.60	1.70	17.10	
	4	7	41.20	3.30	24.63	
	3	9	1.20	.33	.04	
	3	8	3.27	.53	.13	
	3	7	40.30	3.30	26.68	
	3	6	46.10	5.60	37.56	
	2	6	3.50	1.10	.48	
						19.202
^{208}Pb						
1050 A MeV[a]	6	11	128.00	22.00	106.46	
	6	10	10.90	1.70	.54	
	5	11	149.00	25.00	120.13	
	5	10	51.00	18.00	83.37	
	4	10	10.90	1.80	5.04	
	4	9	22.20	3.70	19.68	
	4	7	37.80	4.70	28.02	
	3	9	1.76	.81	.05	
	3	8	4.90	1.60	.16	
	3	7	45.20	4.80	30.36	
	3	6	51.00	13.00	42.94	
	2	6	7.30	2.70	.55	
						42.293

Table 4. Concluded

Target	Fragment charge	Fragment mass number	Experiment cross section, mb	Experiment uncertainty, mb	NUCFRG2 cross section, mb	Chi square per degree of freedom (n)
^{208}Pb						
2100 A MeV[a]	6	11	145.00	17.00	128.19	
	6	10	7.80	1.50	.53	
	5	11	155.00	23.00	153.25	
	5	10	74.00	25.00	82.40	
	4	10	10.00	1.40	4.98	
	4	9	22.50	2.60	19.36	
	4	7	47.90	4.90	27.44	
	3	9	1.43	.53	.05	
	3	8	3.40	.82	.15	
	3	7	45.90	4.60	29.73	
	3	6	60.00	8.50	43.42	
	2	6	4.20	1.10	.55	
						21.363

[a]From references 37 and 39.

Table 5. Chi Square Analysis of Fragmentation Cross Sections of Oxygen Projectile Ions on Targets Other Than Carbon

[See page 39 for footnote]

Target	Fragment charge	Fragment mass number	Experiment cross section, mb	Experiment uncertainty, mb	NUCFRG2 cross section, mb	Chi square per degree of freedom (n)
^{9}Be						
2100 A MeV[a]	8	15	43.00	2.20	57.60	
	8	14	1.60	.10	.60	
	7	15	54.10	2.70	57.80	
	7	14	49.50	4.00	63.00	
	7	13	8.01	.40	7.04	
	7	12	.66	.05	.33	
	6	14	5.21	.30	11.10	
	6	13	28.60	1.40	48.20	
	6	12	60.80	4.90	40.91	
	6	11	21.00	1.10	6.08	
	6	10	2.81	.17	.21	
	5	13	.50	.04	.41	
	5	12	2.75	.15	4.36	
	5	11	27.50	1.40	32.95	
	5	10	19.20	1.50	33.02	
	4	10	3.92	.27	1.99	
	4	9	9.79	.50	9.91	
	4	7	22.00	1.10	16.83	
	3	7	27.00	1.40	18.24	
	3	6	33.50	2.70	26.60	
						5.722
^{27}Al						
2100 A MeV[a]	7	15	66.00	4.30	69.48	
	6	14	6.29	.46	12.59	
	6	13	31.40	2.00	55.56	
	5	12	3.61	.24	5.03	
	5	11	31.00	1.60	37.64	
	4	9	11.22	.68	11.34	
	3	7	34.80	1.80	21.12	
						3.021
^{63}Cu						
2100 A MeV[a]	8	15	74.00	7.80	85.47	
	8	14	2.14	.42	.78	
	7	15	98.20	9.80	92.10	
	7	14	72.00	14.00	82.02	
	7	13	14.70	1.60	9.22	
	7	12	.42	.18	.43	
	6	14	7.76	.92	14.45	
	6	13	35.80	3.70	63.11	
	6	12	92.00	14.00	53.65	
	6	11	27.00	2.60	7.91	
	6	10	4.45	.52	.27	

Table 5. Continued

Target	Fragment charge	Fragment mass number	Experiment cross section, mb	Experiment uncertainty, mb	NUCFRG2 cross section, mb	Chi square per degree of freedom (*n*)
^{63}Cu						
2100 A MeV[a]	5	13	0.82	0.17	0.54	
	5	12	2.98	.38	5.72	
	5	11	35.90	2.90	42.91	
	5	10	35.20	5.50	42.64	
	4	11	.30	.13	.21	
	4	10	6.51	.86	2.57	
	4	9	12.30	1.10	12.94	
	4	7	32.00	2.50	21.79	
	3	8	3.63	.47	.11	
	3	7	38.70	2.90	23.60	
	3	6	61.20	7.90	33.87	
						14.183
^{107}Ag						
2100 A MeV[a]	8	15	99.00	13.00	108.69	
	8	14	2.20	.58	.85	
	7	15	121.00	15.00	123.72	
	7	14	68.00	23.00	89.42	
	7	13	18.60	2.20	10.16	
	7	12	1.11	.34	.47	
	6	14	7.50	1.30	15.75	
	6	13	39.40	5.10	69.55	
	6	12	104.00	18.00	58.14	
	6	11	37.80	3.80	8.70	
	6	10	4.20	1.20	.30	
	5	13	.65	.28	.60	
	5	12	4.04	.58	6.20	
	5	11	43.60	3.90	47.16	
	5	10	26.60	6.30	47.09	
	4	10	5.65	.77	2.84	
	4	9	13.80	1.50	14.16	
	4	7	36.40	3.20	23.80	
	3	7	39.80	3.50	25.79	
	3	6	49.40	8.50	38.06	
						12.336
^{208}Pb						
2100 A MeV[a]	8	15	135.00	22.00	162.79	
	8	14	2.80	1.50	.96	
	7	15	202.00	26.00	199.79	
	7	14	71.00	22.00	100.65	
	7	13	17.00	3.20	11.48	
	6	14	12.30	2.20	17.73	
	6	13	45.40	8.30	78.53	
	6	12	126.00	25.00	66.34	
	6	11	36.90	5.70	9.90	
	6	10	7.20	1.40	.34	

Table 5. Concluded

Target	Fragment charge	Fragment mass number	Experiment cross section, mb	Experiment uncertainty, mb	NUCFRG2 cross section, mb	Chi square per degree of freedom (n)
^{208}Pb						
2100 A MeV[a]	5	13	0.70	0.44	0.68	
	5	12	3.98	.75	7.07	
	5	11	52.90	5.90	53.67	
	5	10	35.70	11.00	52.95	
	4	10	6.80	1.10	3.20	
	4	9	15.30	2.10	16.36	
	4	7	43.30	6.40	27.84	
	3	7	39.70	4.30	30.17	
	3	6	56.00	13.00	42.04	
						17.217

[a]From references 37 and 39.

Table 6. Chi Square Analysis of Fragmentation Cross Sections of Argon Projectile Ions on Targets Other Than Carbon

[See page 41 for footnote]

Target	Fragment charge	Fragment mass number	Experiment cross section, mb	Experiment uncertainty, mb	NUCFRG2 cross section, mb	Chi square per degree of freedom (*n*)
KCl						
1650 A MeV[a]	17	34	17.00	10.00	6.05	
	17	35	38.00	15.00	33.26	
	17	36	6.80	3.80	57.01	
	17	37	42.00	31.00	41.18	
	17	39	56.00	29.00	87.56	
	16	31	1.90	1.50	1.23	
	16	32	20.00	6.30	7.08	
	16	33	41.00	8.50	33.54	
	16	34	50.00	11.00	47.23	
	16	35	32.00	8.60	26.56	
	16	36	29.00	6.00	5.35	
	16	37	19.00	4.10	1.40	
	16	38	9.90	2.70	.18	
	15	29	.42	.33	1.33	
	15	30	7.40	1.70	8.53	
	15	31	21.00	3.80	33.93	
	15	32	25.00	3.00	40.25	
	15	33	22.00	5.70	17.64	
	15	34	2.10	1.50	3.27	
	15	35	2.80	.93	.71	
	15	36	.20	.07	.07	
	14	27	1.40	.60	1.42	
	14	28	15.00	2.80	10.41	
	14	29	38.00	5.20	33.97	
	14	30	43.00	5.20	34.70	
	14	31	14.00	9.00	11.70	
	14	32	1.50	1.80	2.11	
	14	33	.54	.89	.37	
	14	34	.16	.10	.03	
	13	25	.86	.44	1.53	
	13	26	8.00	1.30	12.57	
	13	27	37.00	4.30	33.54	
	13	28	18.00	4.70	29.91	
	13	29	22.00	5.30	7.66	
	13	30	1.50	.49	1.38	
	13	31	.58	.32	.19	
	12	23	.40	.18	1.62	
	12	24	21.00	3.50	14.83	
	12	25	26.00	3.90	33.08	
	12	26	29.00	3.20	25.24	
	12	27	10.00	4.70	4.93	
	12	28	.42	.80	.90	

Table 6. Concluded

Target	Fragment charge	Fragment mass number	Experiment cross section, mb	Experiment uncertainty, mb	NUCFRG2 cross section, mb	Chi square per degree of freedom (*n*)
KCl						
1650 A MeV[a]	12	29	0.68	0.34	0.09	
	11	21	.76	.80	1.84	
	11	22	12.00	2.20	17.37	
	11	23	30.00	5.90	31.67	
	11	24	19.00	4.30	20.60	
	11	25	5.20	2.90	3.17	
	11	26	1.70	1.40	.57	
	10	19	.46	.24	2.16	
	10	20	14.00	3.30	19.69	
	10	21	25.00	4.50	30.40	
	10	22	16.00	2.70	16.52	
	10	23	5.50	1.70	1.98	
	10	24	1.40	.51	.35	
	9	18	5.80	2.00	21.65	
	9	19	16.00	3.30	29.02	
	9	20	9.10	1.90	12.66	
	9	21	4.60	1.70	1.30	
	9	22	2.20	.93	.20	
	8	15	2.00	1.10	3.02	
	8	16	24.00	6.10	23.14	
	8	17	17.00	3.80	27.18	
	8	18	8.30	2.50	9.26	
	8	19	6.10	1.40	.86	
	8	20	.99	.30	.11	
	7	13	1.20	.76	3.57	
	7	14	12.00	5.30	24.04	
	7	15	27.00	7.00	26.01	
	7	16	7.70	3.10	6.44	
	7	17	4.80	.73	.56	
	6	10	.48	.55	.16	
	6	11	1.50	.67	4.16	
	6	12	14.00	6.00	24.66	
	6	13	13.00	4.20	24.42	
	6	14	4.00	2.70	4.23	
	6	15	2.80	.98	.35	
	5	9	1.20	.88	1.89	
	5	10	5.60	1.80	24.83	
	5	11	11.00	3.70	22.55	
	5	12	1.60	1.70	2.63	
	5	13	1.90	2.00	.21	
						14.886

[a]From reference 21.

Table 7. Chi Square Analysis of Fragmentation Cross Sections of Iron Projectile Ions on Targets Other Than Carbon

[See page 45 for footnotes]

Target	Fragment charge	Fragment mass number	Experiment cross section, mb	Experiment uncertainty, mb	NUCFRG2 cross section, mb	Chi square per degree of freedom (*n*)
^{7}Li						
1880 A MeV[a]	25		141.00	18.00	187.66	
	24		98.00	7.00	127.29	
	23		88.00	7.00	104.06	
	22		75.00	6.00	89.86	
	21		67.00	6.00	79.78	
	20		64.00	6.00	72.48	
	19		56.00	5.00	66.76	
	18		55.00	6.00	61.97	
	17		38.00	4.00	57.78	
	16		56.00	6.00	54.16	
	15		57.00	6.00	50.95	
	14		57.00	5.00	47.82	
	13		50.00	5.00	45.25	
						2.973
^{9}Be						
1880 A MeV[a]	25		156.00	21.00	186.66	
	24		111.00	9.00	126.30	
	23		88.00	9.00	103.18	
	22		83.00	9.00	88.97	
	21		77.00	8.00	79.10	
	20		68.00	7.00	71.98	
	19		65.00	7.00	66.03	
	18		54.00	7.00	61.34	
	17		54.00	7.00	57.35	
	16		63.00	8.00	53.52	
	15		57.00	8.00	50.33	
	14		75.00	8.00	47.23	
	13		50.00	7.00	44.68	
						2.338
^{27}Al						
1569 A MeV[b]	25		174.04	4.46	210.00	
	24		127.60	3.23	137.75	
	23		91.05	2.70	113.32	
	22		84.12	2.58	97.92	
	21		73.41	2.40	87.22	
	20		68.92	2.31	79.57	
	19		52.89	2.01	73.26	
	18		52.72	2.01	68.26	
	17		45.24	1.85	64.01	
	16		52.27	1.98	60.22	
	15		43.47	1.80	56.78	
	14		58.21	2.08	53.58	

Table 7. Continued

Target	Fragment charge	Fragment mass number	Experiment cross section, mb	Experiment uncertainty, mb	NUCFRG2 cross section, mb	Chi square per degree of freedom (*n*)
^{27}Al						
1569 A MeV[b]	13		45.37	1.82	50.85	
	12		51.76	1.94	48.17	
	11		45.23	1.81	46.10	
	10		49.11	1.88	43.75	
						2.354
^{32}S						
1880 A MeV[a]	25		250.00	22.00	219.02	
	24		128.00	16.00	140.59	
	23		86.00	16.00	115.73	
	22		64.00	10.00	100.47	
	21		91.00	13.00	89.77	
	20		97.00	14.00	81.95	
	19		55.00	21.00	75.66	
	18		74.00	13.00	70.46	
	17		66.00	14.00	66.35	
	16		74.00	12.00	62.24	
	15		50.00	8.00	58.95	
	14		106.00	14.00	55.66	
	13		78.00	18.00	52.98	
						7.376
^{63}Cu						
1569 A MeV[b]	25		238.96	6.78	265.32	
	24		147.44	3.73	158.74	
	23		98.89	3.00	132.79	
	22		98.45	2.97	116.63	
	21		73.64	2.57	105.32	
	20		80.32	2.67	97.14	
	19		59.98	2.31	90.85	
	18		61.18	2.32	85.56	
	17		49.41	2.09	81.17	
	16		59.58	2.27	77.52	
	15		49.82	2.08	74.04	
	14		72.20	2.48	70.87	
	13		51.47	2.10	68.46	
	12		61.03	2.27	66.09	
	11		50.17	2.06	64.08	
	10		54.55	2.14	62.03	
						4.867
^{63}Cu						
1880 A MeV[a]	25		219.00	20.00	268.30	
	24		149.00	16.00	158.27	
	23		121.00	15.00	132.58	
	22		101.00	14.00	116.20	
	21		100.00	15.00	105.34	
	20		98.00	14.00	97.25	

Table 7. Continued

Target	Fragment charge	Fragment mass number	Experiment cross section, mb	Experiment uncertainty, mb	NUCFRG2 cross section, mb	Chi square per degree of freedom (n)
^{63}Cu						
1880 A MeV[a]	19		88.00	14.00	90.84	
	18		95.00	15.00	85.56	
	17		86.00	13.00	81.40	
	16		56.00	11.00	77.47	
	15		88.00	15.00	74.00	
	14		72.00	11.00	70.95	
	13		179.00	27.00	68.58	
						15.432
^{107}Ag						
1880 A MeV[a]	25		280.00	23.00	341.73	
	24		218.00	21.00	170.26	
	23		117.00	15.00	143.15	
	22		124.00	16.00	126.07	
	21		104.00	13.00	114.45	
	20		118.00	14.00	105.98	
	19		79.00	11.00	99.32	
	18		84.00	14.00	93.97	
	17		79.00	14.00	89.40	
	16		96.00	13.00	85.33	
	15		64.00	13.00	81.89	
	14		158.00	20.00	78.77	
	13		112.00	19.00	76.30	
						10.746
^{181}Ta						
1880 A MeV[a]	26		56.00	82.00	659.47	
	25		457.00	34.00	472.04	
	24		206.00	22.00	184.56	
	23		150.00	19.00	156.03	
	22		152.00	19.00	137.52	
	21		129.00	18.00	125.26	
	20		107.00	17.00	116.49	
	19		111.00	20.00	109.34	
	18		100.00	18.00	103.61	
	17		101.00	18.00	99.05	
	16		109.00	17.00	94.48	
	15		133.00	20.00	91.22	
	13		81.00	14.00	85.37	
						44.585
^{208}Pb						
1563 A MeV[b]	25		500.52	13.42	491.81	
	24		223.00	6.18	189.75	
	23		130.18	4.64	159.71	
	22		135.00	4.67	141.33	
	21		104.01	4.11	128.57	
	20		98.20	3.98	119.27	

Table 7. Concluded

Target	Fragment charge	Fragment mass number	Experiment cross section, mb	Experiment uncertainty, mb	NUCFRG2 cross section, mb	Chi square per degree of freedom (n)
^{208}Pb						
1563 A MeV[b]	19		79.76	3.60	112.27	
	18		77.23	3.54	106.34	
	17		59.97	3.14	101.80	
	16		75.75	3.47	97.07	
	15		63.66	3.19	93.81	
	14		86.28	3.65	90.52	
	13		61.90	3.12	87.75	
	12		74.14	3.38	85.15	
	11		66.19	3.20	83.33	
						5.457
^{208}Pb						
1880 A MeV[a]	25		509.00	40.00	522.88	
	24		242.00	25.00	189.22	
	23		142.00	20.00	159.56	
	22		148.00	22.00	141.41	
	21		111.00	17.00	128.62	
	20		144.00	22.00	119.33	
	19		90.00	19.00	112.31	
	18		73.00	15.00	106.64	
	17		90.00	19.00	101.65	
	16		116.00	19.00	97.65	
	15		78.00	16.00	93.67	
	14		119.00	22.00	90.71	
	13		191.00	37.00	87.82	
						13.641
^{238}U						
1880 A MeV[a]	25		646.00	43.00	582.03	
	24		208.00	22.00	193.87	
	23		181.00	27.00	163.80	
	22		95.00	16.00	144.57	
	21		153.00	21.00	132.02	
	20		143.00	19.00	122.79	
	19		105.00	15.00	115.3	
	18		113.00	19.00	109.7	
	17		133.00	22.00	104.7	
	16		116.00	22.00	100.2	
	15		176.00	34.00	96.56	
	14		169.00	28.00	93.24	
	13		307.00	79.00	90.97	
						52.651

[a]From reference 34.
[b]From reference 20.

Table 8. Chi Square per *n* Values for Target and Projectile Atomic Numbers

	Chi square per *n* for Z_P of—									
Z_T	5	6	7	8	10	11	12	13	18	26
3										3.0
4		11.0		5.8						2.3
6	6.5	6.2	7.8	7.6	8.1	11.0	11.5	5.3	6.8	5.0
13		13.7		3.0						2.3
16										7.4
18									14.9	
29		23.6		14.2						10.2
47		19.3		12.3						10.7
73										44.9
82		31.5		17.2						21.2
92										52.7

REPORT DOCUMENTATION PAGE

Form Approved
OMB No. 0704-0188

1. AGENCY USE ONLY *(Leave blank)*	2. REPORT DATE	3. REPORT TYPE AND DATES COVERED
	October 1995	Technical Paper

4. TITLE AND SUBTITLE
NUCFRG2: An Evaluation of the Semiempirical Nuclear Fragmentation Database

5. FUNDING NUMBERS
WU 199-45-16-11

6. AUTHOR(S)
J. W. Wilson, R. K. Tripathi, F. A. Cucinotta, J. L. Shinn, F. F. Badavi, S. Y. Chun, J. W. Norbury, C. J. Zeitlin, L. Heilbronn, and J. Miller

7. PERFORMING ORGANIZATION NAME(S) AND ADDRESS(ES)
NASA Langley Research Center
Hampton, VA 23681-0001

8. PERFORMING ORGANIZATION REPORT NUMBER
L-17470

9. SPONSORING/MONITORING AGENCY NAME(S) AND ADDRESS(ES)
National Aeronautics and Space Administration
Washington, DC 20546-0001

10. SPONSORING/MONITORING AGENCY REPORT NUMBER
NASA TP-3533

11. SUPPLEMENTARY NOTES
Wilson, Cucinotta, and Shinn: Langley Research Center, Hampton, VA; Tripathi: University of Southern Illinois, Carbondale, IL; Badavi: Christopher Newport University, Newport News, VA; Chun: Old Dominion University, Norfolk, VA; Norbury: University of Wisconsin, LaCrosse, WI; Zeitlin, Heilbronn, and Miller: Lawrence Berkeley Laboratory, Berkeley, CA.

12a. DISTRIBUTION/AVAILABILITY STATEMENT
Unclassified–Unlimited
Subject Category 93
Availability: NASA CASI (301) 621-0390

12b. DISTRIBUTION CODE

13. ABSTRACT *(Maximum 200 words)*
A semiempirical abrasion-ablation model has been successful in generating a large nuclear database for the study of high charge and energy (HZE) ion beams, radiation physics, and galactic cosmic ray shielding. The cross sections that are generated are compared with measured HZE fragmentation data from various experimental groups. A research program for improvement of the database generator is also discussed.

14. SUBJECT TERMS
Cosmic ray shielding; Nuclear cross sections; Radiation protection

15. NUMBER OF PAGES
47

16. PRICE CODE
A03

17. SECURITY CLASSIFICATION OF REPORT	18. SECURITY CLASSIFICATION OF THIS PAGE	19. SECURITY CLASSIFICATION OF ABSTRACT	20. LIMITATION OF ABSTRACT
Unclassified	Unclassified	Unclassified	